CHART Scientific Report 2021

FCC-ee Injector Study and the P^3 Project at PSI

P. Craievich, M. Schaer, N. Vallis, R. Zennaro

on behalf of the CHART FCC-ee Injector collaboration

May 2022

This report gives an insight into the progress of the FCC-ee Injector CHART Collaboration within the past 12 months. The report is organized with one section per work package in order to highlight the results obtained for every topic. Some organizational aspects are described right at the beginning.

Contents

1 Coordination and Overall Parameter Optimization (WP0)

The FCC-ee Injector Study is a collaboration between PSI and CERN with some external partners, such as CNRS-IJCLab (Orsay), BINP (Novosibirsk), INFN-LNF (Frascati) and SuperKEKB (Tsukuba, interested in the P-cubed project at PSI as an observer). Figure 1 shows the Work Breakdown Structure (WBS) with the division of the project activities into work packages and the responsible laboratories. The project has two deliverables:

- the review of the CDR0 published in 2019 [1] including a cost estimate and the proof of principle positron source and capture system, and
- the PSI Positron Production (P^3 or P-cubed) project at PSI.

The cost estimation will start as soon as the technologies of the linacs and of the positron source will be defined. The SwissFEL linac cost model will be the starting point for the estimation.

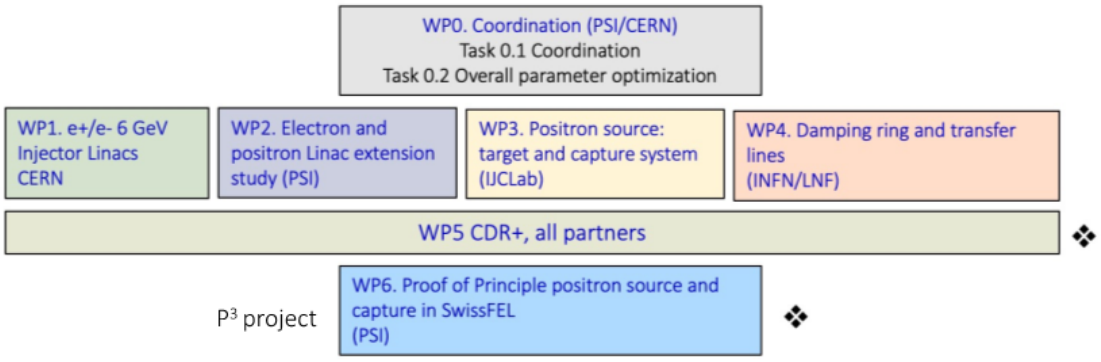

Figure 1: The Work Breakdown Structure (WBS) with the division of the project activities into work packages and the responsible laboratories.

The FCC-ee injector complex must provide beam for top-up injection in the two rings of the Future Circular Collider (FCC) supporting a beam lifetime of about 1 hour on Z pole and as low as 12 minutes at high energy. It must also allow for a filling from zero (alternating bootstrapping injection) within at most half an hour. The baseline described in the FCC-ee CDR [1] considers a 6 GeV linac, with at most 2 bunches per RF pulse, with a repetition rate up to 200 Hz. In this scheme, portions of the same linac were used for multiple purposes, similarly to the SuperKEKB injector set up [2]. Alternative scenarios have meanwhile been proposed, considering three different aspects:

- The number of bunches per pulse can be increased by an order of magnitude, while the linac repetition rate can be slightly reduced to provide an overall much faster filling time. The price to pay is a larger damping ring, more challenging positron production requirements, additional constraints on the linac, and possibly (much)

less flexibility in pulse-by-pulse, bunch-by-bunch intensity control required for top-up operation.

- A different layout allows some of the lower energy linacs to be separated from the main linac which accelerates the bunches before the injection into the pre-booster or booster ring.
- The pre-booster ring could be replaced by an extension of the main linac to 20 GeV (or even 45 GeV), possibly with C-band RF accelerating structures instead of S-band.

At the beginning of the year 2021, the study focused on a revision of the new injector layout. The option of accelerating a train of bunches has been considered, differently from the only two bunches proposed in the CDR0. In April 2021, a review meeting with international experts was organized in order to compare the two options and receive guidelines for the injector design [3]. During the review meeting, the optimum layout and linac operation mode were also discussed. The focus was on the operational stability, reliability and availability as central requirements on the injector, as well as sufficient flexibility, taking into account the specific needs of the collider, especially for top-up injection. The following list reports the most significant guidelines from the review report [3], which have been followed for our further studies:

1. Adopt new layout for 6 GeV with only one energy in each linac and positron production at 6 GeV;
2. Linac RF frequencies should be chosen to be an appropriate multiple of the FCC-ee collider RF frequency, currently 400 MHz, to make potential future injection operation much easier to perform;
3. Check the acceptance of the booster ring in terms of emittance because this parameter will greatly influence the injector itself, i.e. RF guns and damping ring;
4. Carry out start-to-end simulations for the new baseline layout;
5. Rough relative cost comparison for new and old layout (probably only marginal differences);
6. Concentrate on 2-bunch per pulse conservative scheme as recommended by review, with positron target inspired by SLC's [4];
7. Study of 6-to-20 GeV linac, including rough cost estimate;
8. Positron source performance at electron beam energy of 20 GeV;
9. Consolidation and confirmation of positron yields expected at 6 and 20 GeV;
10. Preparation of PSI positron experiment (P^3 project) based on a target compatible with 2-bunch operation.

Few iterations have followed the review meeting to finalize the specifications for the injection into the booster ring. Two possible scenarios have been identified for the injector complex, as depicted in Figure 2.

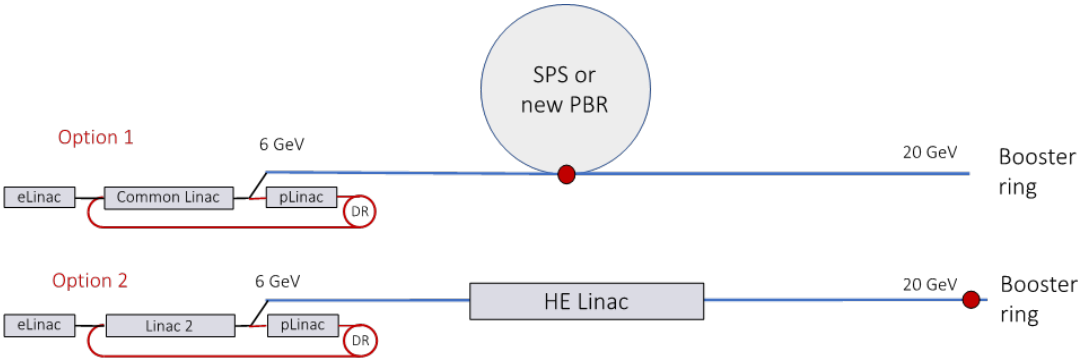

Figure 2: Two main scenarios for the injector complex: (1, top) the baseline, where the 6 GeV beams are injected into a pre-booster ring (possibly the already existing SPS at CERN) and (2, bottom) the high-energy (HE) variant, where a linac boosts the energy up to 20 GeV for direct injection into the booster ring.

The first scenario remains the baseline, where the 6 GeV beams are injected into the existing Super Proton Synchrotron (SPS) ring or into a new pre-booster ring (PBR). In the second option, an additional high-energy (HE) linac would boost the energy from 6 GeV to 20 GeV and inject the beams directly into the main booster. The injector complex up to 6 GeV can be identical in the two scenarios. Table 1 lists the target parameters at the end of the injector complex for the two options.

Table 1: Target parameters for the two main scenarios of the injector complex: the baseline and the high-energy (HE) linac.

Scenario	Baseline	HE Linac
Ring for injection	PBR	BR
Injection energy [GeV]	6	20
Bunch population 10^{10} (nC)	3.47 (5.55)	3.12 (5.0)
Repetition rate [Hz]	200	200
Number of bunches	2	2
Bunch spacing [ns]	15, 17.5, 20	15, 17.5, 20
Rms normalized emittance (x, y) [mmmrad]	50, 50	50, 50
Rms bunch length [mm]	1	1
Rms energy spread [%]	0.1	0.1

Another important topic over the past year has been the filling scheme of the colliders in order to get an estimate of the filling times and to get an idea of the timing of the whole injector. Figure 3 shows a schematic layout with the necessary cycles to fill the colliders from scratch. The 12 cycles for each species are designated to pre-compensate the charge loss due to collisions, and to always keep the charge imbalance within ±5 %,

this operation mode is referred to as bootstrapping [5]. The times necessary for the accumulation and ramping up in the different stages of the injection are listed in Table 2 and also reported in Figure 3.

Table 2: Times required for the filling from scratch of the collider rings for the most demanding Z-mode for the two injector options, linac beam energy up to 6 GeV and 20 GeV, respectively.

Baseline Scenario		**HE Linac Scenario**	
(1) Injector up to 6 **GeV**		**(1) High-energy linac up to** 14 – 20 **GeV**	
Bunch charge = 5.55 nC		Bunch charge = 5.00 nC	
2 bunches per RF pulse at 200 Hz		2 bunches per RF pulse at 200 Hz	
(2) SPS or pre-booster ring		(This step is removed in this scenario)	
Bucket charge = 5.00 nC (90 % transm. from 1)			
Accumulation of 755 bunches	1.89 s		
Emittance cooling (damping time = 0.03 s)	0.1 s		
Ramp up and down time (6 – 20 GeV)	0.28 s		
SPS cycle time	2.29 s		
(3) Top-up booster		**(2) Top-up booster**	
Bucket charge = 4.50 nC (90 % transm. from 2)		Bucket charge = 4.50 nC (90 % transm. from 1)	
Accumulation of 9060 bunches (12 SPS cycle times)	27.48 s	Accumulation of 9600 bunches	24 s
Emittance cooling (damping time = 0.1 s)	0.4 s	Emittance cooling (damping time = 0.1 s)	0.4 s
Ramp-up time (20 – 40.5 GeV)	0.63 s	Ramp-up time (20 – 40.5 GeV)	0.63 s
BR cycle time	28.53 s	BR cycle time	25.03 s
(4) Collider		**(3) Collider**	
Bucket charge = 40.5 nC		Bucket charge = 40.5 nC	
10 BR injections per specie of 4.50 nC (90 % transm. from 3)		10 BR injections per specie of 4.50 nC (90 % transm. from 2)	
Total filling time Z- mode	570.6 s	Total filling time Z- mode	500.6 s
Luminosity lifetime	1089 s	Luminosity lifetime	1089 s

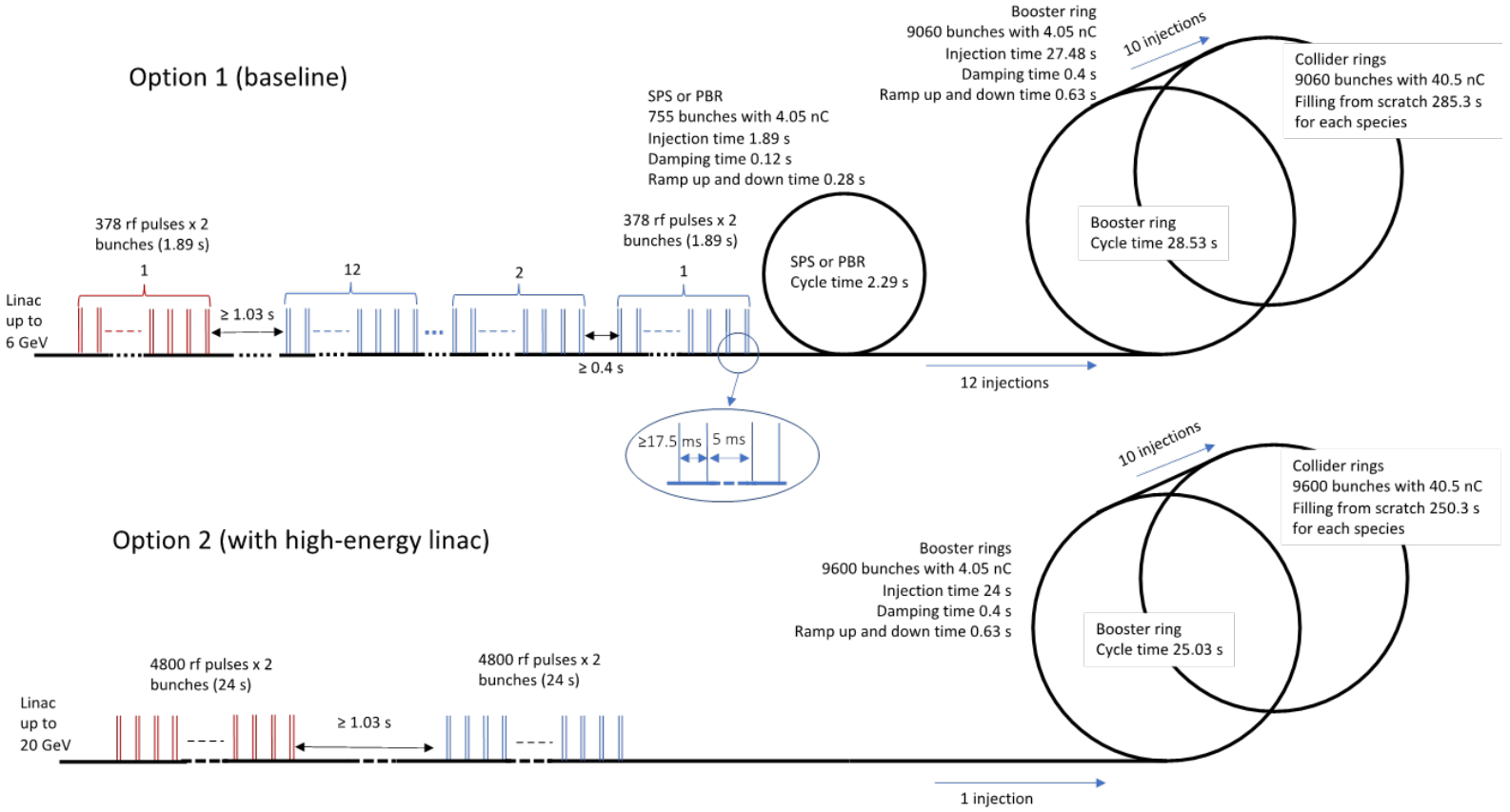

Figure 3: Schematic of the layout, for the two options, with the number of bunches and cycle times to fill the collider from scratch. Considering a transmission efficiency in the injector of 85 % the required charge for both species is 4.8 nC.

2 Electron Source, Electron and Positron Linacs (WP1, WP2)

The latest baseline layout of the FCC-ee injector complex is shown in Figure 4. It foresees two separate linacs for electrons and positrons up to a beam energy of 1.54 GeV – the eLinac and the pLinac, respectively. An advantage of this layout is that the solenoidal channel for the positrons in the pLinac can be extended without interruption beyond the exit energy of the former injectors (about 200 MeV in the CDR0 baseline). Switching to a FODO lattice at a larger energy can potentially increase the achievable positron yield and – at the same time – simplify the linac layout. As we will see in section 2.2, it might eventually be possible to directly switch from a solenoidal channel to a conventional FODO lattice, despite the huge emittance of the positron beam.

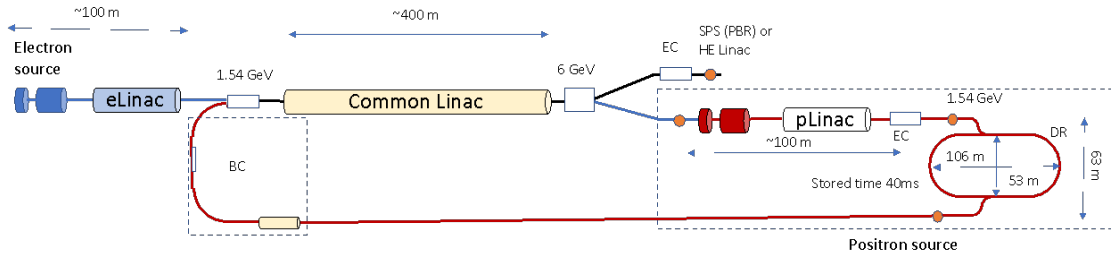

Figure 4: Latest baseline layout of the FCC-ee injector complex.

At the energy of 1.54 GeV, the positron beam is injected into the damping ring, where its emittance decreases to the level necessary for the injection into the pre-booster ring (PBR) or booster ring (BR). The energy of both species is then further boosted in the common linac up to 6 GeV, which corresponds to the input energy for the PBR.

To ensure that the collider is filled on time in the Z-mode, the three linacs have to work at a repetition rate of at least 200 Hz. During positron production, the common linac must accelerate positrons and electrons simultaneously. The two options under study for the time structure are shown schematically in Figure 5. In the first option, positrons and electrons are accelerated in two different RF buckets separated by 2.5 ms, implying a repetition rate of 2×200 Hz $= 400$ Hz. This has an impact on the RF source, the klystron and the accelerating structures, which all must be able to operate at such high repetition rate and correspondingly large dissipated power. These aspects are under investigation. In the second option, the two positron and two electron bunches are accelerated in the same RF pulse. Allocating four bunches in one RF pulse is very challenging for the low-level RF system and the feasibility of this approach must be well investigated. An even more fundamental problem would be the necessity of different magnets' settings for electrons and positrons.

In this chapter, the different parts and systems of the injector complex are introduced, with an emphasis on the most critical points that have been studies up to know.

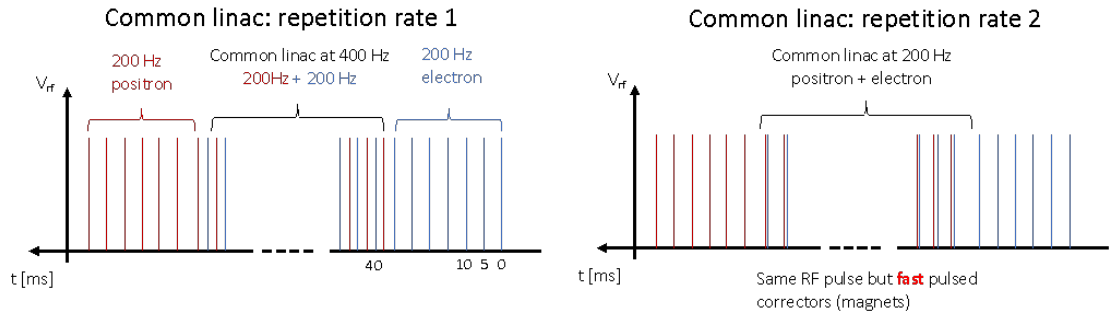

Figure 5: Two options for the time structure of the common linac: (left) 400 Hz repetition rate with either two electron or two positron bunches per RF pulse and (right) 200 Hz repetition rate with two electron and two positron bunches per RF pulse.

2.1 Electron Source

2.1.1 Operation Modes

The latest baseline layout of the injector complex (see Figure 4) foresees a single electron source for the two main operation modes:

- production of the electron beam for the collider and
- production of the electron drive beam for positron production.

With the very large yield obtained from the latest developments on the positron source based on an HTS AMD (see section 3), the generation of the electron beam for the collider has become the most demanding mode from the point of view of the charge. The bunch charge required for the (electron and positron) beams going to the collider is in fact 5.55 nC for the baseline scenario (no high-energy linac, see Table 1), against max. 4.8 nC for the drive beam for positron production. The last value has been extrapolated from Table 6 – which summarizes the results for the old required bunch charge of 3.4 nC – taking the new required bunch charge of 5.55 nC, dividing by the lowest yield of 2.3 appearing in the table, and multiplying with the common safety factor of 2. The main specifications for the electron source are collected in Table 3 (before last column).

2.1.2 Beam Specs Already Achieved with First Optimizations

A first conceptual design of the electron source exists and is based on the SwissFEL RF photoinjector depicted in Figure 6 [6].

The results of the first optimizations of the photoinjector for the FCC-ee injector complex are presented in Table 3. Note that this study was performed based on the old collider specifications, requiring a bunch charge of 3.4 nC. New simulations with the latest nominal charge of 5.55 nC (in the option without high-energy linac) still need to be performed.

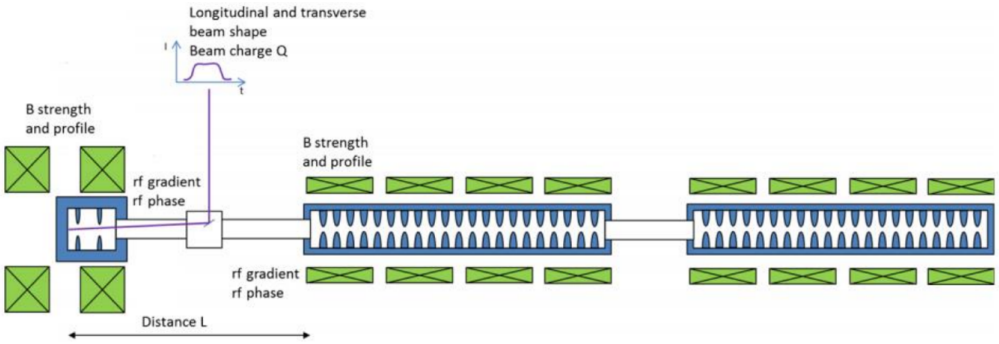

Figure 6: Layout of the SwissFEL RF photoinjector with S-band RF gun and TW accelerating structures (blue) surrounded by solenoids (green). Electrons are extracted from the cathode with a UV laser.

In the simulations with a bunch charge of 3.4 nC, the achieved normalized transverse emittance < 10 mmmrad is well below the required 15 mmmrad, implying that a damping ring is not necessary for the electron beam. This key point must verified also for a bunch charge of 5.55 nC, since it can have a major impact on the whole injector complex.

Table 3: Optimized injector parameters (top part), corresponding simulated electron beam parameters (bottom part) and comparison with the overall machine specifications (second last column). (*) The required charge of the drive beam depends on the performance (yield) of the positron source. (**) Number of simulated bunches. There is currently no show stopper to operate with 2 bunches.

Mode	e- beam for collider	e- beam for collider	e- drive beam for e+ production	Specs.
Frequency [GHz]	3	3	3	-
Electric field at cathode [MV/m]	100	100	100	-
Transv. laser spot distr.	Uniform	Gaussian	Uniform	-
Initial spot size (rms) [mm]	1.2	0.8	1.5	-
Laser pulse length [ps]	15 (FWHM)	4.5 (rms)	15 (FWHM)	-
Gun solenoid field [T]	0.2413	0.245	0.2413	-
TW acc. gradient [MV/m]	16.2	10	16.2	-
Pos. first TW structure [m]	1.068	0.78	1.068	-
Beam energy [MeV]	206	187	206	200
Bunch charge e- collider [nC]	3.4	3.4	-	3.4
Bunch charge e+ production [nC]	-	-	5	(*)
Norm. emittance (rms) [mmmrad]	1.94	8.2	3.1	< 15
Bunch length (rms) [mm]	1.4	1.6	1.4	$1 - 2$
Relative energy spread [%]	0.4	0.6	0.4	< 1
Beam size (rms) [mm]	1	1	0.7	
No. of bunches	1 (**)	1 (**)	1 (**)	2
Bunch distance [ns]				> 17.5
Charge stability [%]				3
Repetition rate max. [Hz]				200

2.2 Positron Linac Between Injector and Damping Ring

2.2.1 Large Positron Emittance

Independently from the above discussion, the studies up to 1.54 GeV have focused on the acceleration and transport of the positron bunch. Its main characteristics are a huge transverse emittance and energy spread in comparison to conventional electron beams, in the order of 10000 mmmrad and 15 % respectively. Table 6 collects the main parameters of the positron bunch at the end of the positron injector (for different setups up to about 200 MeV). The design of the positron linac is currently focusing on the transport of the distributions obtained with the AMD, which provides considerably higher yields.

2.2.2 Possible Sections of the Positron Linac

The design of the positron linac up to 1.54 GeV is a work in progress where several aspects still have to be studied in detail, including their interconnections. The main design goal is the transport of the whole positron beam – say with losses at least < 10 % – provided by the injector. In the following paragraphs we briefly summarize the results already achieved and the steps planned to complete a first realistic design.

As depicted in Figure 7, three main types of section have been identified for the positron linac:

- Section 1 (green): solenoids around the RF accelerating structures;
- Section 2 (red): FODO lattice with quadrupoles around the RF accelerating structures;
- Section 3 (blue): FODO lattice with quadrupoles between the RF accelerating structures.

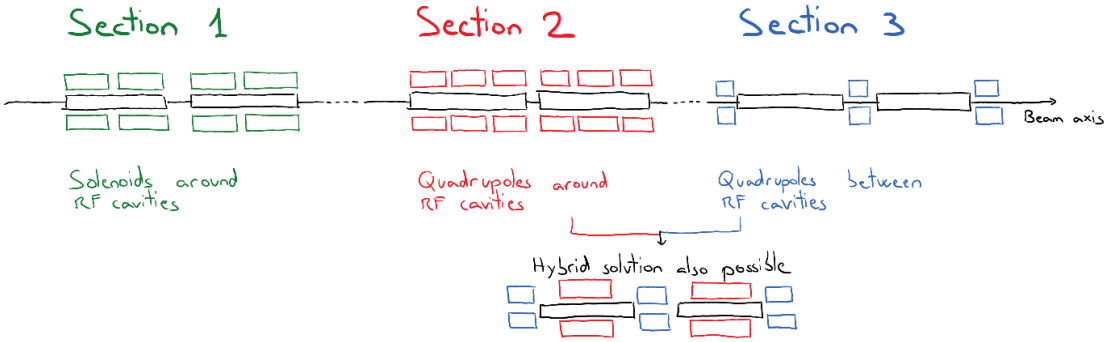

Figure 7: Subdivision of the positron linac up to 1.54 GeV in different sections: (1) solenoids around, (2) quadrupoles around and (3) quadrupoles between the RF accelerating structures.

It is under investigation which types of section are necessary and the optimal beam energy at the transitions. The numbering from 1 to 3 indicates the expected sequence with the increasing beam energy.

2.2.3 Basic Transverse Dynamics in a FODO Lattice (Sections 2 and 3)

In a first phase, the studies have focused on the transverse dynamics of the positron beam with very large emittance. Well-known analytical formulae describing FODO lattices in the thin lens approximation have been very useful to investigate the large parameter space (note that these formulae assume a mono-energetic beam, meaning that the large energy spread is neglected in these considerations). It became soon clear that a conventional FODO lattice cannot be started at 200 MeV with an already relatively large radial aperture of 20 mm of the irises of the RF TW structures. The iris aperture, together with the transverse emittance and the beam energy, defines the maximum (and consequently the minimum) acceptable beta function of the FODO lattice. The length of the FODO cell and its quadrupole spacing are then maximized by choosing a phase advance of 76.35 deg. The quadrupole spacing must be maximized because it is in the order of only few tens of centimeters at the lowest energies considered, as demonstrated by Figure 8.

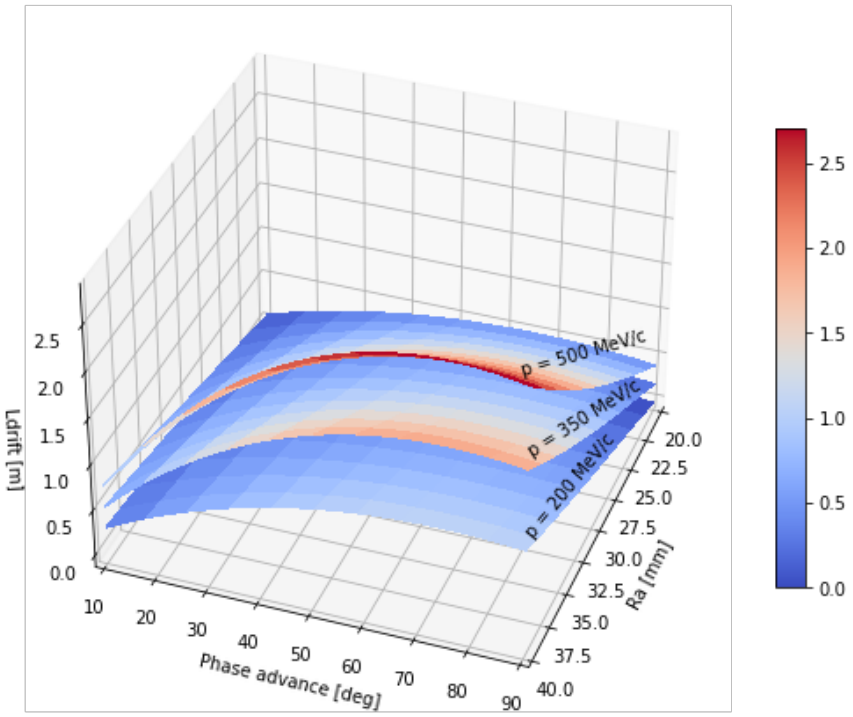

Figure 8: Quadrupole spacing (length of the drift space Ldrift, z-axis) as a function of FODO phase advance (x-axis) and of the radial aperture of the irises of the RF accelerating structures (y-axis) for different beam momenta (surfaces).

With such small quadrupole spacing, one definitely needs to consider the option of placing very large aperture quadrupoles around the RF accelerating structures, as already done in other studies [1] ("Section 2" in Figure 7). According to PSI magnets' experts, such quadrupoles with pole fields well below 1 T are feasible but big and relatively costly. One advantage is that the length of the RF accelerating structures is not limited by the FODO lattice.

From above 1 GeV, a more conventional FODO lattice with the quadrupoles between the RF accelerating structures ("Section 3" in Figure 7) seems to be feasible. This solution restricts the maximal allowed length for the RF structures – and very probably their efficiency – to the spacing between quadrupoles (minus some margin) dictated by the FODO lattice.

Figure 9 proposes an example of a design for linac sections 2 and 3, where the transition between section 1 and 2 has been chosen at 500 MeV and that between section 2 and 3 at 1 GeV. Corresponding values are listed in Table 4.

Table 4: Parameters corresponding to the example design of Figure 9. The parameters in the first part of the table remain constant for a certain FODO cell, while those in the second part vary along the FODO.

	Parameter	Section 2		Section 3	
Constant along FODO	R_a [mm]	30		30	
	F_a [mm]	4		4	
	$\epsilon_{n,x}$ [πmmmrad]	10000		10000	
	Ψ [deg]	76.345		76.345	
	β_+ [m]	5.504		11.008	
	β_- [m]	1.299		2.599	
	L_{cell} [m]	3.305		6.611	
	f [m]	1.337		2.674	
	L_{quad} [m]	1.000		0.350	
	k_{quad} [1/m2]	0.748		1.068	
	R_{pole} [mm]	100		35	
	L_{drift} [m]	0.653		2.955	
	E_{acc} [MV/m]	15		15	
	$L_{section}$ [m]	33.333		33.333	
	# Quads	22		10	
Variable along FODO		Start	End	Start	End
	E [MeV]	500	1000	1000	1500
	σ_+ [mm]	7.500	5.303	7.500	6.124
	σ_- [mm]	3.644	2.577	3.644	2.975
	G_{quad} [T/m]	1.247	2.495	3.564	5.346
	B_{pole} [T]	0.1247	0.2495	0.1247	0.1871

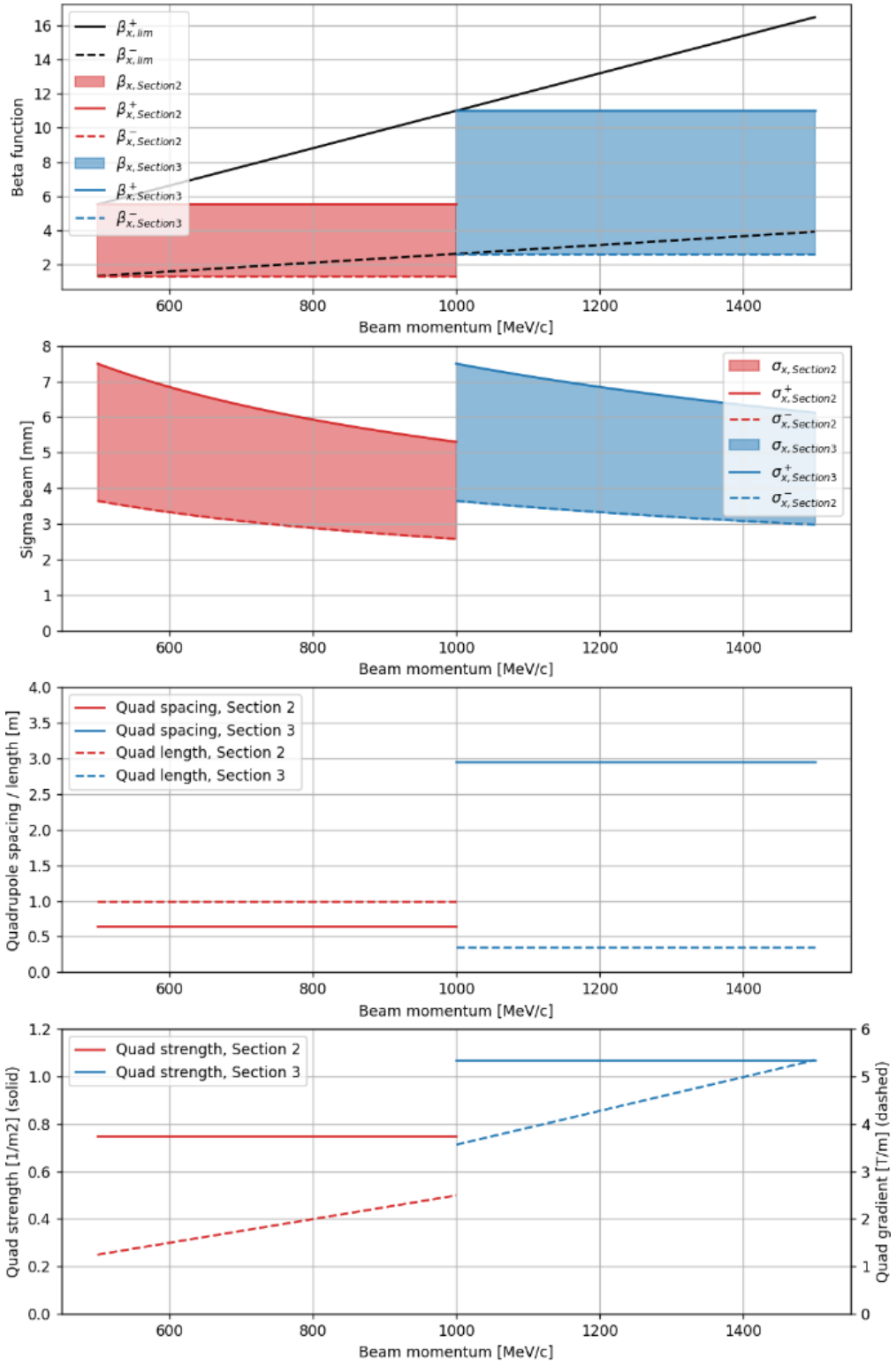

Figure 9: Beta function, transverse rms beam size quadrupole spacing and length (3rd plot) and quadrupole strength and gradient (4th plot) for a design example of linac sections 2 (red) and 3 (blue). The beam beta function and beam size would oscillate within the colored areas along the FODO lattice, limited by the max. (solid lines) and min. (dashed lines) values.

2.2.4 Up to which Energy Can we Push the Solenoids (Section 1)?

We have just shown that all tools are mature to make concrete proposals for the design of the FODO sections of the positron linac. Before going further with this analysis, we need to study in detail the first section of the linac, where the transverse size of the beam is contained by the solenoidal channel. In particular, we must understand up to which energy we can transport the beam with the solenoids and which field strength is required.

From the simulations performed in the framework of WP3 (see section 3) and WP6 (see section 5) we know that the positron beam can be transported in a solenoidal channel up to about 200 MeV with an excellent capture efficiency. A small separation of the solenoids providing a near-to-constant solenoidal field is a key point to ensure a large capture efficiency in the injector linac (see section 5.5.3). This aspect needs now to be seriously considered in the simulations of the positron injector studied in WP3, where for the moment a simple homogeneous solenoidal field has been modeled after the AMD. The effect gets weaker as the beam energy increases. We expect therefore to be able to transport the positron beam with solenoids and minimal losses from about 200 MeV.

This is supported by preliminary simulations with RF-Track [8] showing an extension of Section 1 up to the target energy of 1.54 GeV, which fulfills the goals in terms of transport efficiency (see Figure 10). This seems to be possible even with a longitudinal magnetic field on-axis of 0.5 T, which could be provided by (conventional but large) normal conducting solenoids. In the simulation of Figure 10, a decent capture efficiency of about 90 % between 200 MeV and 1.5 GeV is achieved with an almost vanishing solenoidal field in the middle between the RF accelerating structures. These fields are the result of a separation of 0.2 m between the RF accelerating structures and 0.3 m between the solenoids. In a more realistic design, the separation of the solenoids should be further increased to provide enough space for the RF couplers. This would sharpen the valleys in the solenoidal field, which generally affect the capture efficiency. Fortunately, we are very confident that these valleys can be smoothen out by increasing the separation between RF structures and adding an additional, small solenoid between the output coupler of one structure and the input coupler of the next one. A more constant solenoidal channel and a better capture efficiency (near to 100 %) than those presented here are finally expected.

While the positron distribution is very near to a Gaussian distribution in both transverse phase spaces, more interesting is the longitudinal phase space reported in Figure 11. It is characterized by a large bunch length and energy spread. The observed filamentation is already present at 200 MeV and still visible after the linac at 1.5 GeV. It is compatible with other studies (independent and using different simulation codes) [7] but is not yet understood. Since only the main filament – containing the majority of the charges – is observed at 200 MeV in other simulations, this aspect will be studied in detail.

Inspired by the HTS (High-Temperature Superconducting) technology of the adiabatic matching device (AMD), the possibility to use HTS solenoids also around the RF accelerating structures is being investigated. For this purpose –where increasing

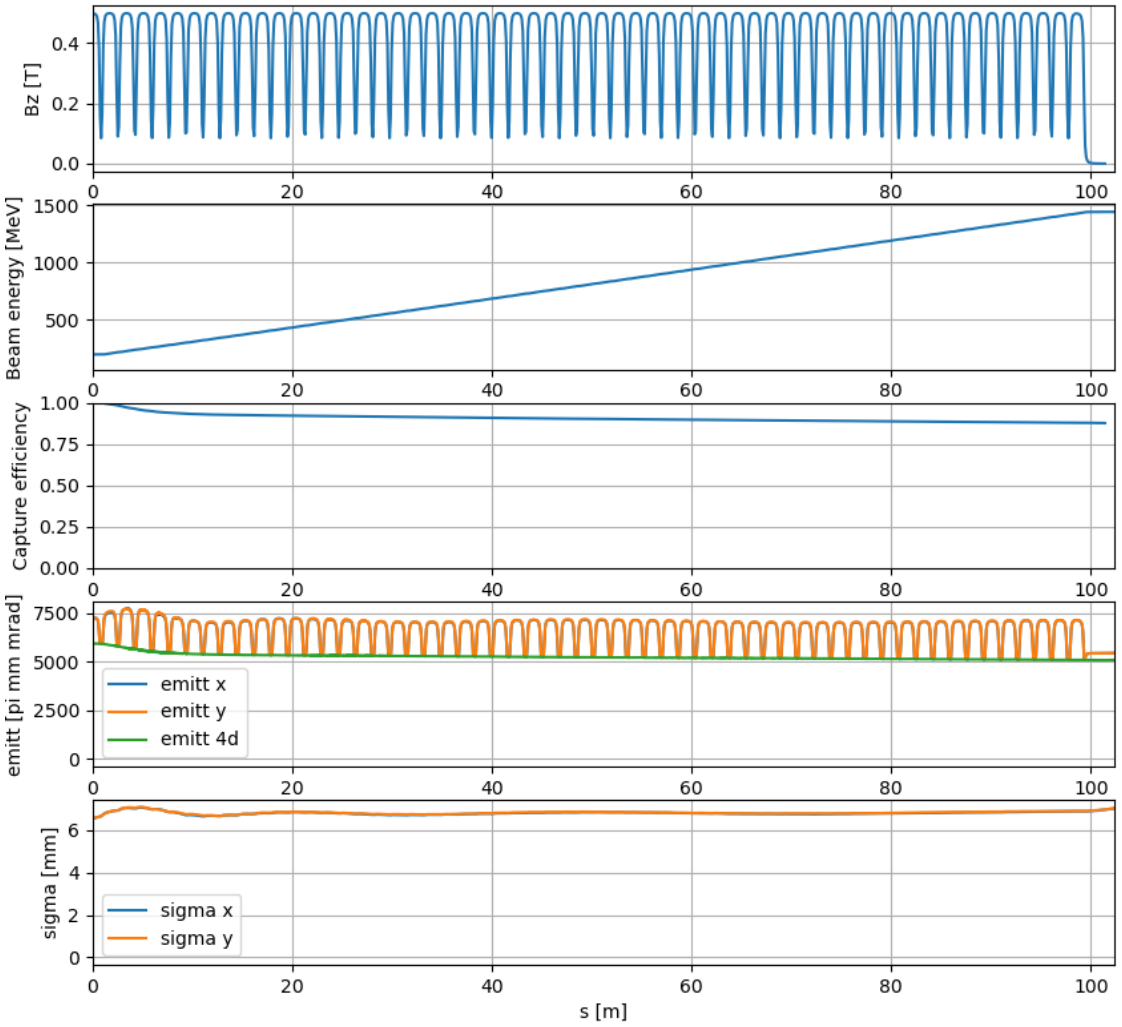

Figure 10: Preliminary simulation of a positron linac boosting the energy from 200 MeV up to about 1.5 GeV and guiding the beam with the only help of solenoids (i.e. only the section type 1 of Figure 7 is used). Beam line setup: 58×1.5 m long CLIC TW L-band structures at 15 MV/m surrounded by one 1.4 m long solenoid each.

the solenoidal field on-axis beyond 1.5 T does not bring any advantage anymore – the cheaper technology based on MgB_2 superconductors is more interesting than the more expensive REBCO technology of the AMD.

Since the use of solenoids up to this beam energy would represent a non-conventional solution, several aspects related to the robustness of the solution must be studied, among which:

- The effect of beam offsets and angle errors on the trajectory and transport efficiency,

- The possibility to run the linac without steerer magnets and
- Eventual undesired effects and/or simulation inaccuracies due to the very large beam size as compared to the geometric dimensions of the RF accelerating structures.

Particle tracking studies with the software RF-Track (also used to simulate the capture linac) are ongoing.

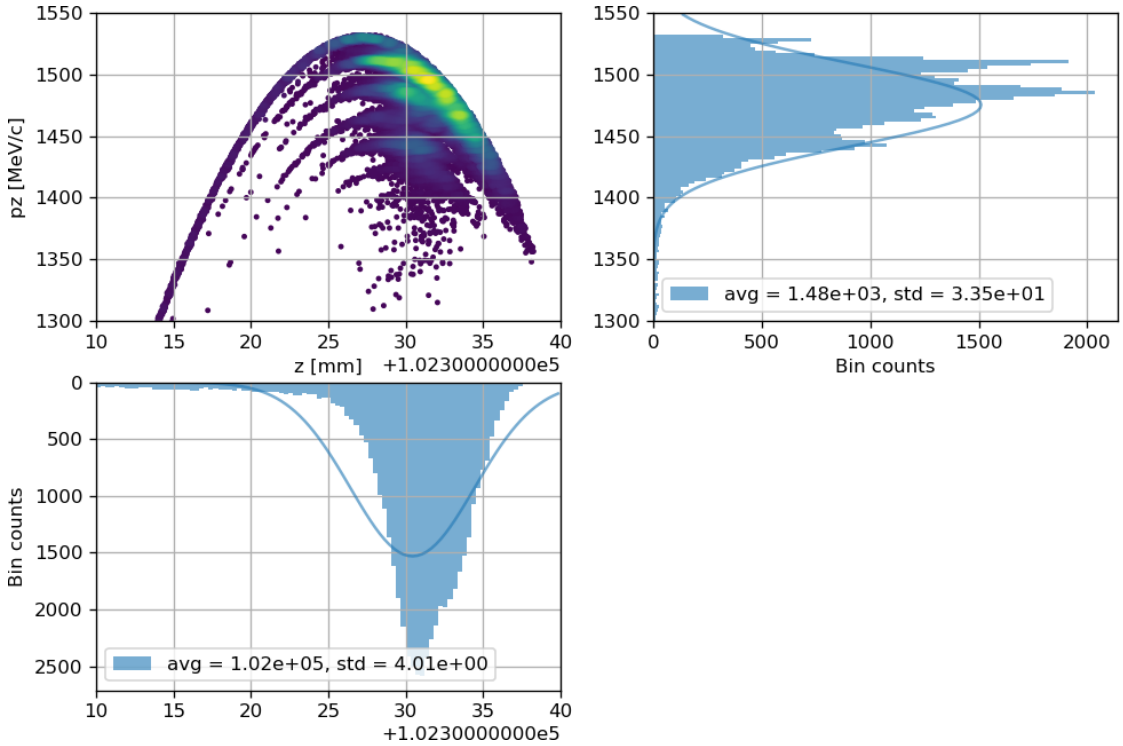

Figure 11: Longitudinal phase space of the (main bucket) of the positron beam at the end of the simulation of Figure 10, i.e. at about 1.5 GeV.

2.2.5 Interplay Between Beam Dynamics and RF Design

For the above computations and simulations, assumptions must be done regarding some parameters of the RF accelerating structures. One key parameter is the minimal radial aperture of the RF accelerating structures. The current value of 30 mm is very large but still meaningful. The RF experts have already proposed viable solutions after optimizing the RF design with this value, as described in section 2.4.1. The requirements of the beam dynamics clearly sets the boundary conditions for the RF design. Several fruitful iterations between beam dynamics and RF experts have already been done and will still be necessary in the near future.

2.2.6 Portion of the Beam Accepted in the Damping Ring

It is very probable that the dynamic aperture of the damping ring will limit the portion of the positron bunch that will be accepted (not lost) in the damping ring itself. Quantitative considerations on this aspect will be possible as soon as a reliable tracking of the transverse (solenoids and/or quadrupoles) and longitudinal (RF structures) plane through the linac up to 1.54 GeV will be available. Applying then the dynamic aperture of the damping ring (computation on going) to the positron distribution coming from the linac will show whether a reiteration of the linac and/or damping ring design will be necessary in order to maximize the positron yield after the damping ring. If certain particles will anyway be lost along the beam line, then it would be better to loose them at an energy as low as possible to avoid unnecessary radiation.

A third harmonic RF structure is being implemented in the RF-Track simulation in order to reduce – and potentially completely compensate for – the correlated energy spread of the positron beam. There is the potential to considerably increase the positron yield after the damping ring (see Figure 11).

The concept of dynamic aperture usually involves the transverse position and the momentum of the particles, assuming that the emittance of the incoming beam is comparable to the equilibrium emittance of the ring. The application of this concept to the damping ring must be reviewed, since the incoming transverse emittance is 3 orders of magnitude larger than the equilibrium emittance. This will be a key point to provide reliable values of the positron yield after the damping ring.

2.3 Electron and Electron/Positron Linacs

The study of:

- the electron linac from the injector ($\sim$ 200 MeV) to the electron/positron linac (1.54 GeV) and
- the electron/positron linac from 1.54 GeV to 6 GeV

has just started and will be reported in the next scientific report. Their design is expected to be less challenging than that of the positron linac up to 1.54 GeV itself, but they of course need to be compatible with and integrated into the overall layout of the injector complex. This corresponds to a remarkable amount of work to be done.

2.4 RF Studies

The studies related to the design of the RF accelerating structures for the different electron and positron linacs are generally very advanced. In particular, a tool has been developed that allows to optimize the RF system based on boundary conditions like the RF power and pulse length available from the source, the chosen frequency and the desired length of the accelerating structures. It has already been mentioned how the requirements from the beam dynamics drive the design of the RF system.

2.4.1 TW Structures for Very Large Emittance Positron Beam

Up to now, the focus has clearly been set on the study of the accelerating structures of the positron linac up to 1.54 GeV. The requirement of a minimal radial aperture around 30 mm (plus/minus few millimeters) is very challenging because it corresponds to a very large iris aperture even at low frequencies (e.g. 2.0 GHz). Smaller radial apertures – e.g. 20 mm as in an initial guess – would not allow for reasonable FODO lattices with a high transport efficiency of the positron beam.

2.4.2 Frequency, Length and Efficiency of Accelerating Structures

A fix point regarding the frequency of the accelerating structures is that it will be a multiple of 400.70 MHz, the RF frequency of the collider ring. Even though the frequencies of the different linacs have not been fixed yet, there are clear tendencies:

- Positron linac up to 1.54 GeV: the requirement of a very large iris aperture currently makes 2.0 GHz the most probable candidate.
- Electron/positron linac from 1.54 GeV to 6 GeV: A good compromise between acceleration efficiency and limited energy spread seems to be 2.8 GHz.
- Electron linac up to 1.54 GeV: 2.8 GHz with the same motivation as above and to limit the number of frequencies in the injector complex.

Figure 12 compares many designs of TW accelerating structures at 2.0 GHz with different length, minimum radial aperture and phase advance. For the variants with a radial aperture of 30 mm (red), the optimum in terms of effective shunt impedance is not very sharp wrt. the structure length (and same phase advance). This permits to choose shorter structures without compromising excessively their efficiency, as e.g. for the case F with a length of 4 m and only about 10 % less efficient than the case D with a length of about 7 m. We recall Figure 9 and Table 4 to remember that in the section 3 of the positron linac (quadrupoles between the accelerating structures) the structure length is limited by the FODO lattice. In the ideal (but unrealistic) case where the structures could be 20 m long, the conventional phase advance of $2\pi/3$ could provide an efficiency 20 % larger than case F.

It is not surprising to note that smaller iris apertures correspond to an improved efficiency. If a minimal radial aperture of 20 mm could be considered, the acceleration efficiency could be approximately doubled at 2.0 GHz (compare cases A–C vs. D–F). Furthermore, one could opt for a higher frequency to further increase the efficiency (results are not presented here but available in a very similar form as Figure 12).

For the selected designs presented in Table 5, we note that the effective shunt impedance of 39 MΣ/m for a 3 m long structure is not very high but not even dramatically low, in particular considering the limited length of the positron linac up to 1.54 GeV as compared to the other linacs of the injector complex. The computations providing the klystron power required by one structure assume an RF pulse of 5 μs from the source which is then compressed with a SLED to match the filling time of the structures in

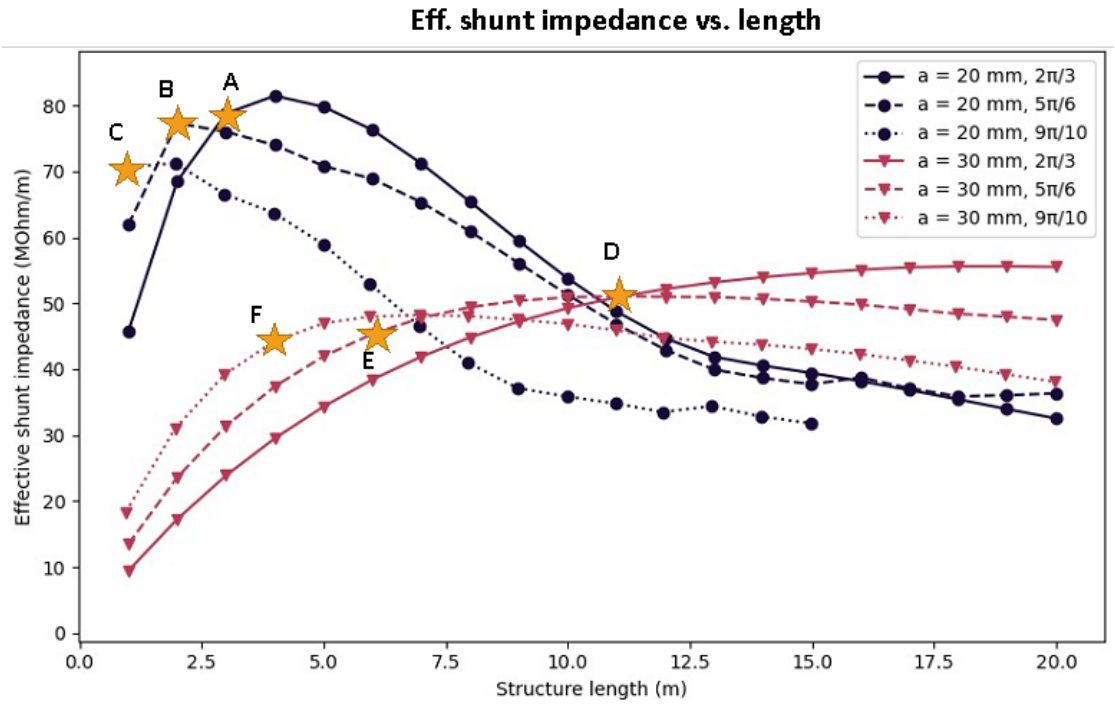

Figure 12: Effective shunt impedance as a function of the length for different designs of the TW accelerating structures at 2.0 GHz. The values in the legend indicate the minimal radial iris aperture and the phase advance per cell of the design. The stars correspond to some interesting candidates with the current requirements from the beam dynamics.

the order of 450 – 600 ns. The generation of an RF pulse of 5 μs at 200 Hz repetition rate is for sure challenging for the source but – according to the feedback from several companies – definitely feasible for the considered RF frequencies. The company CETD stated that they could provide an RF pulse of 5 μs and 80 MW (peak power) at 200 Hz [9].

2.4.3 Reentrant Iris Geometry

After the beam dynamics requirement of a very large aperture, also the shape of the cells for the accelerating structures has been reconsidered. In a first phase, a conventional "SwissFEL-like" geometry has been considered (Figure 13, left). After some parameter sweeps taking into account the given boundary conditions – primarily the large minimal aperture – it turned out that a "reentrant" iris geometry (Figure 13, right) generally brings the following advantages as compared to the SwissFEL-like geometry:

- Higher shunt impedance,
- Shorter accelerating structures,

- Lower modified Poynting vector but larger surface fields and
- Effective high order modes (HOM) detuning.

As we can see from Table 5, the iris thickness is tapered from 14.3 mm for the first cell to 20.0 mm for the last cell. This allows to achieve a constant accelerating gradient along the whole structure by keeping a constant iris aperture.

With the assumption that the RF pulse entering the accelerating structures is shorter than 1 μs, the following high-gradient limits are taken as boundary conditions for the RF design:

- Maximum surface electric field < 100 MV/m and
- Maximum modified Poynting vector < 2300 mW/μm^2.

Table 5: Main parameters of different designs of the RF accelerating structures. These three designs originate from the variant F (star) in Figure 12: (F) 4 m long structure exactly as in Figure 12, (F3) same structure but only 3 m long and (F3 higher gradient) same as (F3) but assuming a higher accelerating gradient. (*) Approximate number of structures required to boost the energy from 200 MeV to 1.54 GeV.

Variant	F	F3	F3 higher grad.
Frequency [GHz]	2.0	2.0	Same geometry
Constant radial aperture [mm]	30	30	
Phase advance [rad]	$9\pi/10$	$9\pi/10$	
Length [m] (num. cells)	4.0 (59)	3.0 (44)	
Entrance, exit iris thickness [mm]	14.3, 20.0	14.3, 20.0	
Transverse wake at 17.5 ns [V/pC/mm/m]	0.13	0.13	
Filling time [ns]	599	447	
Min. group velocity [c]	0.019	0.019	
Largest cell radius [mm]	61	61	
SLED coupling	15	17	
Eff. shunt impedance [MΣ/m]	44	39	
Average gradient [MV/m]	15	15	20
E_{max} (instant.) [MV/m]	62	58	77
$S_{c,max}$ (instant.) [mW/μm^2]	370	329	585
Klystron pulse length [μs]	5	5	same
Klystron power per structure [MW]	20	17	30
Number of structures*	23	30	23

2.4.4 Squared Section to Minimize Quadrupole Aperture

As depicted in Figure 7, it might be necessary to have a linac section where quadrupoles are placed around the RF accelerating structures. The outer diameter of the (usually

cylindrical) structures clearly defines minimal allowed quadrupole aperture. The larger the spacing of the magnetic poles, the more challenging and bulky the magnet design.

A squared transversal section of the accelerating structures (see Figure 14) has the potential to considerably reduce the size and costs of the quadrupoles around them.

To validate the feasibility of this idea, a key aspect to be studied is the cooling of the RF structure. This is basically limited to four cooling channels due to the special geometry. Figure 15 shows a preliminary (steady-state) thermal simulation of the single cell. The results are very promising since a thermal gradient < 2 K is observed between the coldest point in the region of the cooling channel and the hottest point in the region of the iris.

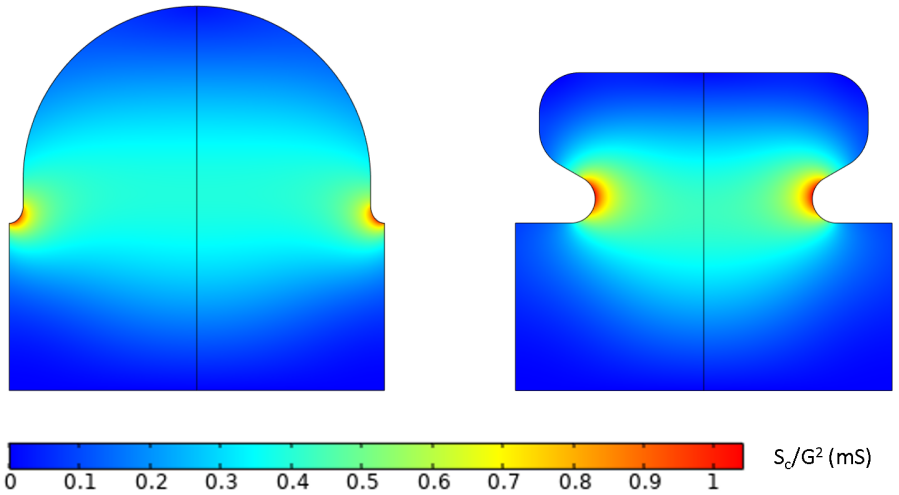

Figure 13: Comparison of different types of cell geometry for the RF accelerating structures of the positron linac up to 1.54 GeV: SwissFEL-like geometry (left) vs. reentrant iris geometry (right). These geometries corresponds to an RF frequency of 2.0 GHz, a radial iris aperture of 30 mm and a phase advance per cell of $9\pi/10$.

2.4.5 TW Structures for Conventional Beam Emittances

The design of the RF system for the electron linac up to 1.54 GeV and of the electron/positron linac from 1.54 GeV to 6 GeV is expected to be less challenging because of the more conventional beam parameters, in particular the much smaller transverse emittance and energy spread. The optimization of the accelerating structures for this linac will be tackled in the near future.

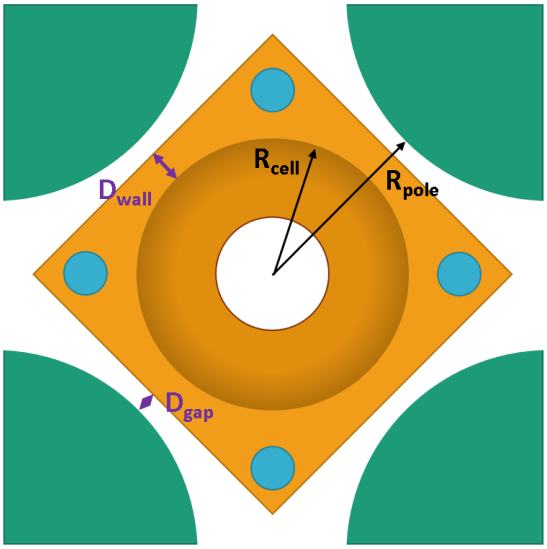

Figure 14: Sketch of the transverse section of an RF accelerating structure with squared section (copper) surrounded by the poles of a quadrupole magnet (green). The idea is to minimize the distance of the magnetic pole R_{pole} from the beam axis by minimizing the wall thickness D_{wall} in the region of the pole and to use the corners for the water cooling (blue). The outer radius R_{cell} of the RF cell and the minimal separation between accelerating structure and magnet D_{gap} are usually given.

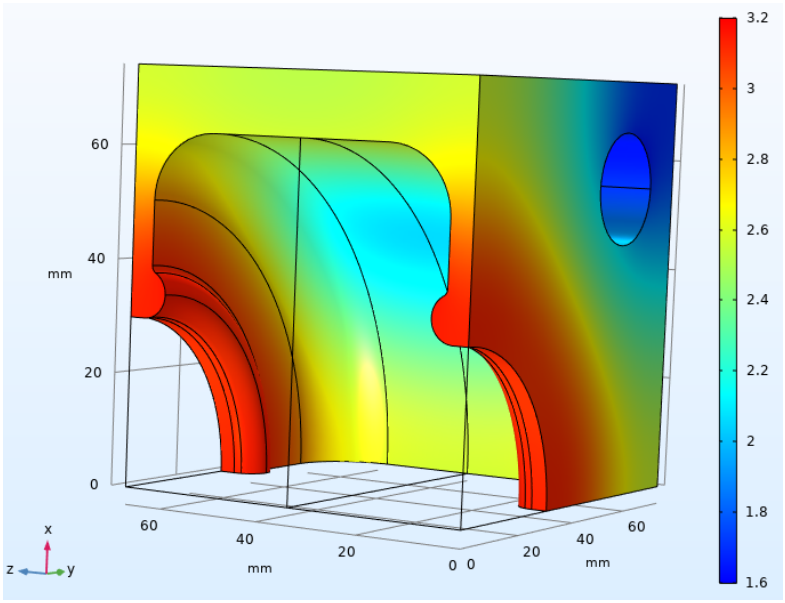

Figure 15: Steady-state temperature rise in K within (one quarter) of the single cell when the accelerating structure is fed with the nominal RF power.

3 Positron Source: Target and Capture System (WP3)

Positron production is always an extremely important topic for any electron-positron collider. This is particularly true for future colliders such as FCC which are designed to operate at the extreme end of parameters where a positron source with a high positron yield is required.

One of the objectives of the CHART project related to the positron source, which aim to contribute to the innovation and development of accelerator concepts beyond existing lepton injector technology, is summarized here: High yield positron production and capture concept with proof of principle. Novel concepts for the production target and positron capture are investigated in theory and experiment with the goal to demonstrate production yield values and efficiencies well beyond present state-of-the-art.

Figure 16 shows the work principle of a conventional positron capture scheme. Electrons from a drive linac hit a small portion of an amorphous target (e.g. tungsten or tungsten alloy) and positrons are created through bremsstrahlung and the following pair conversions. The positron beam is generated with small spatial and temporal distributions, but with large angular (emittance) and energy distributions. This is due to the multiple showering and scattering process and is therefore intrinsically part of the positron generation process. In order to reduce the angular divergence, immediately after the target, the positrons are focused with a strong axial magnetic field in the Adiabatic Matching Device (AMD). The magnetic field is decreased adiabatically and consequently the divergence of the positron beam is also decreased. An introduction a more details on the the positron sources are in [10, 11].

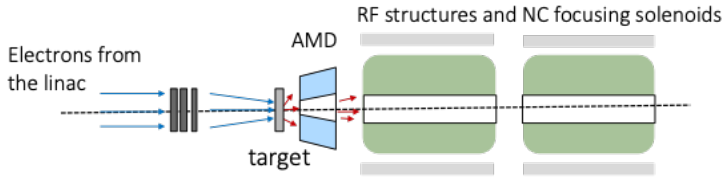

Figure 16: Work principle for a positron capture system.

Two options are considered for the AMD: the first involves the use of a flux concentrator which basically makes use of a pulsed magnet, a technology presently used in the positron source of the SuperKEKB colliders [2] while the second involves the use of a superconducting solenoid (SC). The latter is based on the high-temperature superconducting (HTS) material with which the solenoid coils will be constructed. This is the technology that will also be tested in the SwissFEL experiment at PSI. However, the permissible thermal load as well as thermo-mechanical stresses in the target could limit the power of the primary electron beam. The thermo-mechanical stresses on the target given by the peak energy deposited density (PEDD) and the average heating impose a physical limit to the peak and average positron current for the conventional scheme. To overcome these possible limits imposed by the target in thermo-mechanical terms, a solution using a two-stage process, the so-called hybrid scheme will also be under consideration for a

future study. Figure 17 shows a comparison between the conventional and the hybrid scheme. In the conventional scheme, bremsstrahlung radiation is the main source of photons. To obtain a large number of photons, the electromagnetic shower in the target needs enough thickness (or radiation length) to expand. Thus, the use of axially aligned crystals as radiators can provide better performance than conventional amorphous converters. In this scheme, electrons from the drive linac that penetrate the crystal at radiant angles to the axes or planes are channeled and emit a channeling radiation. This radiation provides a large number of softer photons than bremsstrahlung [12, 13] for the following conventional target.

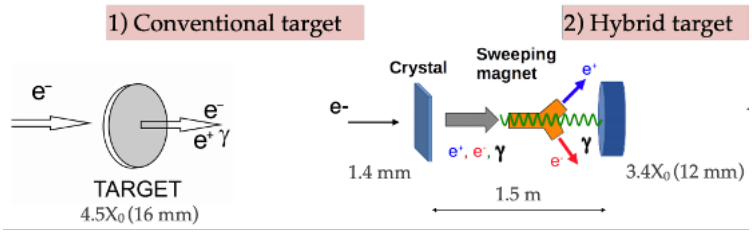

Figure 17: Concept of a conventional and hybrid targets.

However, in the last year we have focused our study on a conventional scheme for the positron source. Table 3 summarizes the results of the simulations carried out in the last year considering both the flux concentrator and the SC solenoid as Adiabatic Matching Device. Furthermore, two working frequencies, 2 and 3 GHz, were considered for the RF structures for positron capture, respectively. The iris diameter was set at 40 mm [14].

Beam dynamic simulations have shown that the flux concentrator can guarantee positron production even with some safety margin. The technology based on a pulsed magnet is well established in other laboratories and has proven to be suitable for FCC-ee as well. The positron source of SuperKEKB is the world's highest intensity positron source currently in operation and is based on the flux concentrator technology and the positron yield, the highest in a running facility, is 0.5 with a repetition rate of 50 Hz. Now it would be important to start the mechanical design including the integration of the target into the flux concentrator and to carry out simulations to define the shielding and thermo-mechanical simulations to define the complexity of the device as a whole. More probable the modification of the current design could be necessary. Operation of the flux concentrator at 100 Hz must be checked experimentally. As far as the current design is concerned, operation at 200 Hz represents an intrinsic difficulty. In this case, design of the flux concentrator should be further developed to allow for 200 Hz operation mode. Eventually, the objectives of this study are to have the reliable and robust design of the positron source for the FCC-ee using the flux concentrator as a matching device (together with the first mechanical integration) and get a cost estimate to be included in the technical design report. An important boundary condition is that the review meeting suggested to continue using the two-bunch scheme as the baseline for the FCCee injector design and a possible promising alternative to the flux concentrator is to use a superconducting (SC) solenoid as a matching device. From the results of the

Table 6: Results of the simulations for two different options of the AMD device and two different options for the capture RF structures.

	Baseline AMD/FC		Alternative AMD/SC sol.			
Drive beam parameters	Value		Value			Unit
Beam energy	6		6			GeV
Numebr of bunch	2		2			
Bunch charge	2.88	2.24	1.43	1.25	1.19	nC
Bunch length (rms)	1		1			mm
Beam size (rms)	0.5		0.5			mm
Bunch separation	>17.5		>17.5			ns
Repetition rate	200		200			Hz
Normalized Emittance	<1		<1			mm.rad
Energy spread (rms)	<1		<1			%
Target parameters						
Tickness	17.5 (5X0)		17.5(5X0)			mm
Beam power	6.9	5.4	3.4	3.0	2.8	kW
PEDD	10.4	8.46	5.58	4.88	4.62	J/g
Deposited power	1.48	1.32	0.88	0.76	0.72	kW
Capture linac parameters						
Frequency range	S-band	L-band	L-band	L-band	S-band	
Iris aperture 2a	30	40	40	40	40	mm
Accelerating gradient	20	17.5/21	17.5/21	17.5/21	18	MV/m
Solenoid strenght	0.7	0.5	0.5	1.5	1.5	T
AMD peak magnetic field	7	7	15	15	15	T
Positron parameters						
Beam energy	198		176			MeV
Bunch charge	6.73		6.73			nC
Positron yield	2.3	3.0	4.7	5.4	5.7	
Bunch length (rms)	2.1		2.2			mm
Normalized emittance (rms)	7.1		11.5			mm.rad
Energy spread (rms)	7.8		17.1			%
Mean energy at DR	1.54		1.54			GeV
Energy Spread at DR (rms)	1.2		1.8			%

latest simulations, it seems that a positron yield even higher than the flux concentrator scheme can be achieved, see table 6. The positron capture simulations are still ongoing and several iterations to be performed between the magnet design, heat load and radiation dose calculations mechanical design and beam dynamics simulations to define the best magnet parameters. The first simulations to estimate the radiation effects on the SC solenoid have also shown promising results regarding the use of the SC magnet in an environment with high radiation losses. On top of that the recent decision to limit the operation mode to two bunches per RF pulse in the injector makes the SC option very attractive. However, this remains a new technology for positron sources and its feasibility and effectiveness should be demonstrated. This is the main purpose of the P-cubed experiment at PSI, together with the studies of the innovative target based on the hybrid scheme.

4 Damping Ring and Transfer Lines (WP4)

The damping ring is necessary to reduce the angular divergence (emittance) of the positron beam to a value appropriate to the injection into the pre-booster or booster ring. The reduction of emittance is achieved through the process of radiation damping, i.e. the combination of synchrotron radiation in bending fields and wigglers with energy gain in RF cavities. The design of the damping ring must ensure a small emittance and a sufficient damping rate. Figure 4 shows a schematic layout with the position of the damping ring and its approximate dimensions. The damping ring is for all intents and purposes part of the positron source because its dynamic aperture, longitudinal and transverse acceptance parameters are the target parameters for the design of the linac and the positron capture. As we already mentioned in paragraph 1, we studied the possibility to increase by an order of magnitude the number of bunches per linac pulse (multi-bunch options) at the expense of a larger damping ring. For this scope a new damping ring was designed in order to accumulate up to 50 bunches. But, relying on review report, the reference design for the DR is again the one published in the CDR. In Table 7 the DR parameters for the 2-bunch and multi-bunch options are listed. The

Table 7: Damping Ring parameters for the 2-bunch and multi-bunch options.

Parameters	2-bunch	Multi-bunch	Unit
Circumference	241.8	268.36	m
Equlilibrium emittance (x/y/z)	0.96/-/1.46	1.34/-/1.71	nm/nm/um
Dipole length, field	0.21/0.66	0.22/0.69	m/T
Wiggler #, length, field	4, 6.64, 1.8	4, 16.6, 1.8	-/m/T
Cavity #, length, voltage	2, 1.5, 4	2, 1.5 m, 4	-/m/MV
Momentum compaction	0.00155253	0.00155253	
Bunch # stored,, charge	16, 3.5	50, 3.5	-/nC
damping time tx/ty/tz	10.5/10.9/5.5	5.65/5.92/3.09	ms
Store time	40	20	ms
kicker rise time @1.54GeV	50	22.5	ns
Energy loss per turn	0.225	0.461	MV
SR power loss wiggler	15.7	90.6	kW

injection time of the 2 bunches must be optimised so that the fast injection kickers do not also affect the stored beam. In addition, the DR should be able to provide the 2.5 ms delay needed for option 1 of the common linac operation. These two aspects impose stringent boundary conditions for the time separation of the two bunches. This specific problem and the definition of the separation in time of the two bunches still need to be investigated and studied in detail. Once these parameters have been defined, the injection and extraction systems will have to be designed and a realistic model of the RF superconducting cavity will have to be also included in order to take into account power dissipation, energy consumption and the total footprint of the cryogenic system. Beam diagnostics and the vacuum system, such as the dimension and shape of the vacuum chamber, will also be important topics to address in order to assess the impact of collective effects on beam dynamics. For this purpose, the estimation of the

impedance budget will be crucial. However, other effects such as intra beam scattering (IBS), Coherent Synchrotron Radiation (CSR) and e-cloud need to be carefully evaluated and may drive further modifications of the vacuum system.

5 PSI Positron Production (P^3) Project (WP6)

5.1 Beam Dynamics Simulations

Most modern positron sources involve a high-Z target hit by a multi-GeV electron beam, which results in a large production of electron-positron pairs [15]. This has been adopted as baseline solution for FCC-ee, where a high-yield positron source is needed. However, the secondary positron distribution is emitted with an extremely wide energy spectrum and large divergence. Therefore, one of the main challenges for the FCC-ee injector is to capture and transport efficiently the positrons produced at the target to the damping ring (DR).

5.1.1 Positron Yield at the Damping Ring

The positron yield refers to the ratio between the populations of secondary positrons and primary electrons at a given point of the accelerator chain. Preliminary simulations for FCC-ee show a yield of $N_{e+}/N_{e-} \approx 13$ at the target exit, but this number is significantly lower in latter stages of the injector due to losses and rejection at different acceptance windows. Therefore, the DR at 1.5 GeV is taken as reference point for calculating the global yield of the system. The damping ring has an acceptance window both in the longitudinal and energy domains. Thus, a good yield at the damping ring needs a high capture efficiency of the linacs, a confined time structure and a low energy spread. A large positron yield is particularly important for future colliders such as FCC which are designed to operate at the extreme end of parameters. The most recent precedent of an operational positron source in an electron-positron collider is at SuperKEKB, based based on a 3 GeV e- drive beam, and providing a yield of $N_{e+}/N_{e-} \approx 0.5$ at the DR. By contrast, the objective for the FCC-ee is to provide a yield of at least $N_{e+}/N_{e-} = 1$ at the DR with a safety factor of 2 [16]. Preliminary simulations by the FCC-ee and P-cubed researchers show yield values around $N_{e+}/N_{e-} = 5$ at the DR. In this chapter, different simulation strategies to estimate the yield and are discussed, and two separate simulation layouts for FCC-ee and P-cubed respectively are introduced.

5.1.2 Simulation Strategy for FCC-ee Capture Linac

While P-cubed is a downsized version of the FCC-ee positron source and capture linac, a full-domain simulation layout is necessary to calculate key parameters like the positron yield. Figure 18 shows the different stages of such simulation. The positron production is simulated with Geant4 [17], a toolkit for of particle-matter interactions. The secondary distribution is plugged into ASTRA [18], a particle tracking code for charged particles under the influence of external EM fields. Such particle tracking is performed along the capture linac: consisting of an adiabatic matching device and 10 RF cavities surrounded by solenoids up to 200 MeV. Finally, no transverse losses are assumed and an algebraic transformation is performed to the beam up to 1.5 GeV, where the particles are filtered with the parameters of the DR acceptance window. With this technique, the value of the yield at the DR as well as detailed information of the beam along the capture

linac (capture efficiency, emittance, energy spread, etc.) is obtained in a relatively quick manner. The results of the latest full-domain simulations are shown in Table 8.

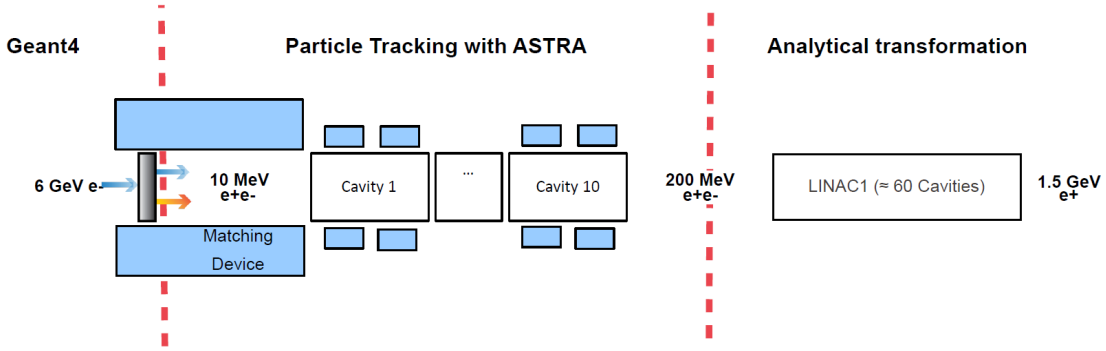

Figure 18: Full-domain simulation strategy from the target to the damping ring.

Table 8: Main beam-dynamics parameters obtained from full-domain simulations

Final energy[1]	197.8	MeV
e+ capture eff.[1]	≈ 75	%
ϵ^1_{norm}	≈ 15000	$\pi\ mm\ mrad$
Energy Spread[1]	≈ 50	MeV
AMD maximum B_z	15.1	T
Solenoid field	1.5	T
Maximum e+ Yield[2]	5.67	

[1]At the end of the capture linac
[2]At the DR

5.1.3 Simulation Strategy for P-cubed

Another simulation layout is used based solely the P-cubed devices. While Geant4 and ASTRA are still used for simulating positron production and tracking, several differences are noticed between Figure 18 and Figure 19. After the target and the AMD, the beam is only tracked along two cavities surrounded by solenoids. A spectrometer is included in the ASTRA simulation and the resulting electron and positron beams are post-processed in order to evaluate the beam diagnostics section.

In Figure 20, the latest simulation results with the P-cubed layout are presented, showing a snapshot of the beam before the separation at the spectrometer.

5.2 Adiabatic Matching Device

Despite the vast positron production at the target, capture and transport of the secondary beam has a great influence on the final yield due to the large emittance and energy spread. In this respect, one of the key elements of our positron source is the

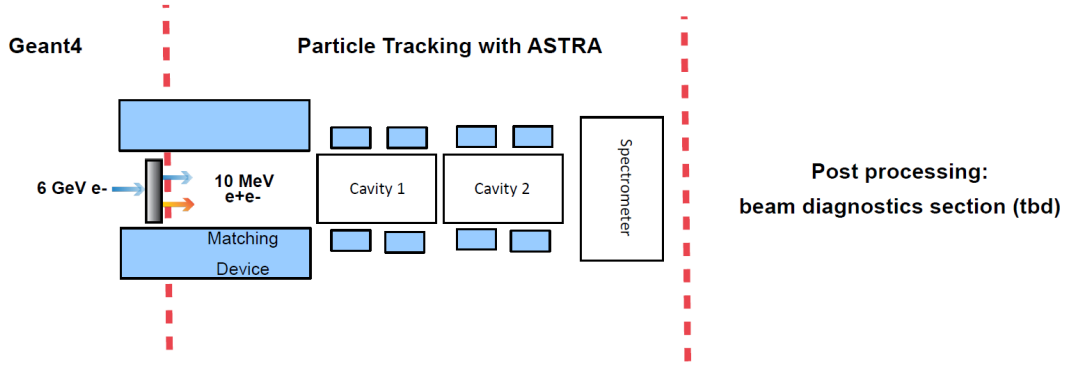

Figure 19: Simulation strategy for P-cubed, from the target to the beam diagnostics section.

adiabatic matching device (AMD), a superconducting solenoid that provides an adiabatically tapered magnetic field around the target exit. It is long known that a strong, adiabatically tapered solenoid can provide higher yields at the damping ring with respect to other common solutions such as the flux concentrator and the quarter-wave transformer. This technique not only confines the highly divergent positrons at the source, but also enhances the energy acceptance at the damping ring, being especially suitable for multi-GeV positron beams with wide energy spectra [19, 20].

5.2.1 Size Optimized HTS Solenoid

The use of a high temperature superconducting (HTS) solenoid has been suggested as technological solution for the AMD. HTS magnets operate at temperatures above 20 K, reducing significantly the space and power consumption required for cooling. More precisely, such solenoids can be implemented with non-insulated ReBCO tape, which does not require a high-temperature or high-pressure treatment and can be assembled in-house at PSI without major technical difficulties. In addition, despite the market price of the ReBCO tape is currently high, a substantial decrease is foreseen for the following years [21]. Initially, an arrangement of 22 HTS coils and a peak field of 17.7 T was proposed by magnet experts at PSI (Figures 21 and 22), providing a positron yields up to 4.7 at the FCC-ee damping ring according to preliminary simulations [22]. However, it also was concluded that the position of the target with respect of the AMD peak field has a great impact on such yield, and further studies by WP3, shown in Figure 22, showed that the optimum position of our target was around 0.2 m downstream from the center of the magnet [23].

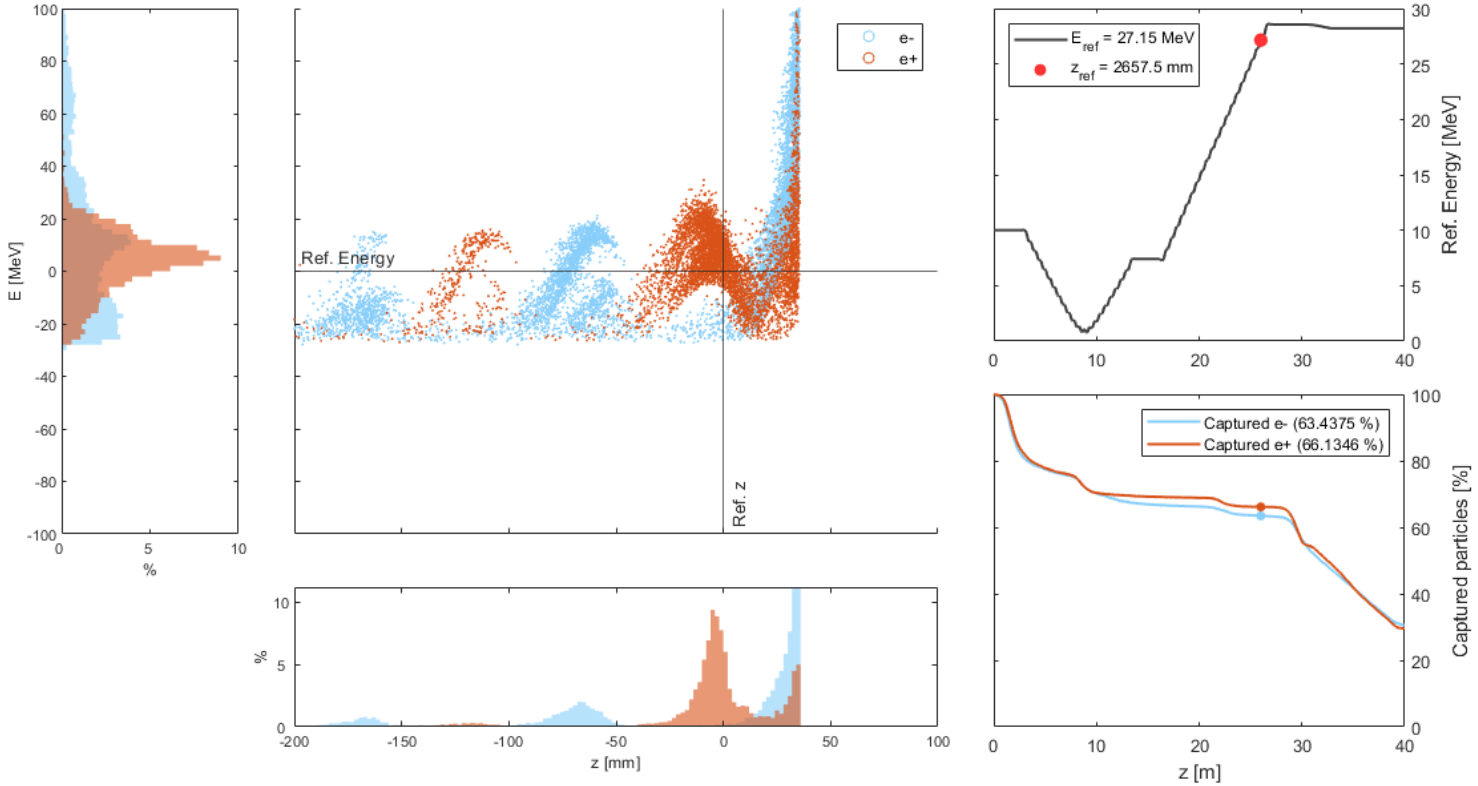

Figure 20: Snapshot of the simulated electron-positron beam after the second cavity.

It can be noted that the most upstream coils provide little or no contribution to the field downstream from the target exit, which is effectively the only region where the positron beam is sensitive to the magnetic field. As shown in Figure 23, such field can be obtained with a significantly smaller number of coils. After several iterations with magnet experts at PSI, a solenoid of 5 HTS coils (Figure 24) was taken as new reference, in pursuit a better compromise between field quality and cost.

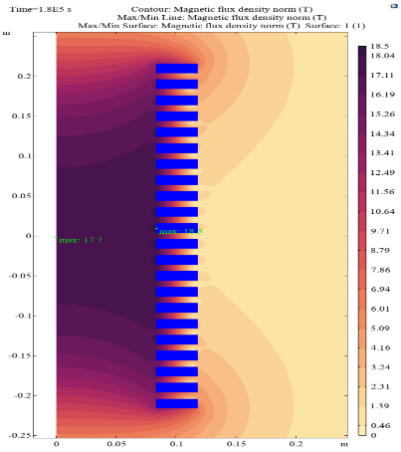

Figure 21: Magnetic field simulation of the original 22-coil HTS solenoid (J. Kosse).

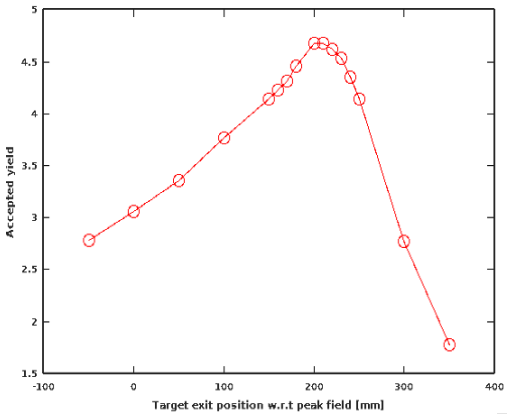

Figure 22: Yield accepted at the FCC-ee DR with respect to target position (Y. Zhao).

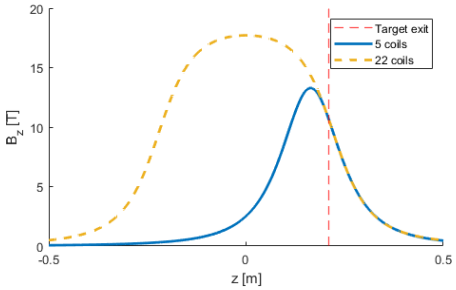

Figure 23: Comparison of the original 22-coil and the downsized 5-coil layouts.

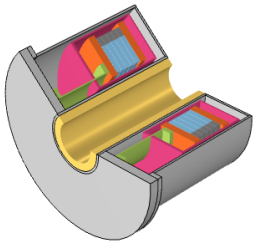

Figure 24: Current baseline design of the AMD (J. Kosse)

5.2.2 AMD Aperture and Target Handling

As seen in Figure 22, the position of the target with respect to the AMD is a critical parameter for the positron yield. Therefore, the experiment must include a mechanical target handling system to study this property in real life. A dedicated handling tool has been proposed to adjust the position of the target on-site. Yet, the aperture size of the AMD strongly depends on the mechanical design of the handling system.

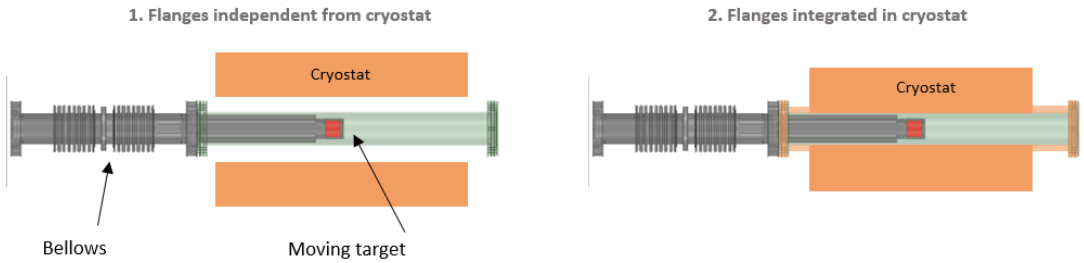

Figure 25: Two options for AMD and target handling system. Left: AMD/cryostat aperture of 72 mm. Right: AMD/cryostat aperture of 38.6 mm with CF flanges part of the cryostat.

There are two baseline approaches currently under discussion regarding mechanical engineering. The first one (Figure 25 left) is based in an AMD/cryostat aperture of 72 mm in order to fully fit an independent vacuum chamber including the two CF40 flanges (70 mm diameter). This solution has several mechanical advantages but requires thicker coils for the same field amplitude on axis. In the second one (Figure 25 right), the AMD is designed with an aperture of 38.6 mm, allowing to use a smaller amount of tape and thus reducing substantially the cost of the experiment. However, this option implies that the two CF40 flanges are part of the cryostat. In addition, it should be noted that a tungsten shielding layer (see yellow layer in Figure 24) may or may not be included, depending on the results of future radioprotection studies.

Table 9: comparison of 5 AMD proposals.

	Bore size	e+ capture provided
Baseline: wide bore[1]	72 mm	63.2%
Wide bore, less conductor	72 mm	61.0%
W.b., l.c., no shielding	72 mm	63.8%
Narrow bore[1]	38.6 mm	65.9%
Narrow bore, no shielding	38.6 mm	65.3%

[1]Cost estimated above WTO tender call limit of 230 kCHF

Considering the two options stated above, five design proposals have been studied. In Table 9, simulations of the yield provided at the FCC-ee damping ring are presented. These results indicate that similar yields can be achieved at a significantly lower cost range with the 38.6 mm bore.

5.3 RF Capture Cavities

The capture of the positron beam into stable RF buckets is provided by a couple of S-band RF cavities, shown in Figure 26. Because of the extremely large transverse emittances, the RF cavity design is based on a standing wave solution that can provide a large iris aperture and transverse acceptance. This kind of solution can also provide a

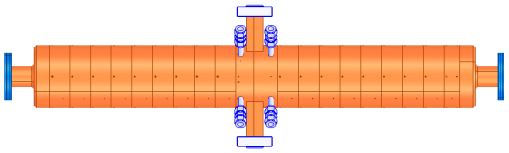

Figure 26: Lateral view of one 1.2-meter S-band standing wave capture cavity.

good RF efficiency without the need of a pulse compressor. The availability of commercial klystrons and conventional waveguide components determined the choice of the 3 GHz frequency for the experiment; instead for the FCC-ee positron injector a frequency in the range between 2 GHz and 2.8 GHz is expected. For the experiment in SwissFEL the coupling factor of the cavities and the total amount of cells per cavities have been defined to optimize the operation for a 3 μs RF pulse length. Each cavity is connected to the waveguide system via a double feeder coupler which is placed centrally in order to increase the mode separation. One single klystron modulator system similar to the one already installed in the SwissFEL injector can provided the required peak power and RF pulse length to fill the two cavities and reach a gradient of 18 MV/m. Even if the experimental repetition rate will be only 1 Hz because of radiation limitation, the cavities have been designed for operating up to 100 Hz, this will reduce the conditioning time. The proper adjustment of the relative phase between the structures will provide the correct bunching condition. A high power in vacuum phase shifter, which is under development at PSI, will be installed and used for this purpose. The main parameters if the cavities are listed in Table 10.

Table 10: Main parameters of the RF standing wave cavities.

Cavity length	1.2	m
Cavity frequency	2.9988	GHz
Operational gradient	18	MV/m
Number of cells	21	
Quality factor	21600	
Shunt impedance	13.9	MΩ/m
Coupling factor	2	
Filling time	3	μs
Mode separation	5.3	MHz
Max. repetition rate	100	Hz

5.4 Tuning of the RF Phases

The positrons are generated at the target with an extremely large divergence and energy spread, but the short bunch length of the primary electron beam is preserved (see Figure 27). The picture is slightly different after the positrons pass through the AMD. In the transverse plane, particles with the highest transverse momentum are quickly lost, reducing the overall divergence of the beam. The surviving particles are then confined

by the AMD, which preserves the resulting transverse emittance. As for the longitudinal plane, no significant decrease of the energy spread is observed, and a large longitudinal dispersion is introduced by the AMD due to spiraling (Figure 28).

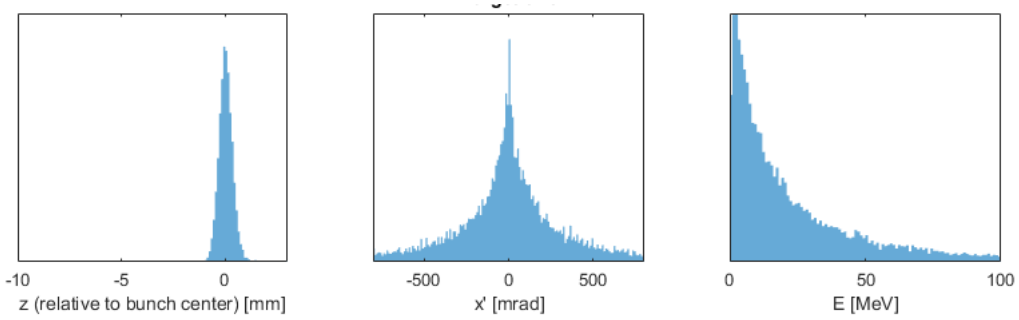

Figure 27: Positron distribution at target exit.

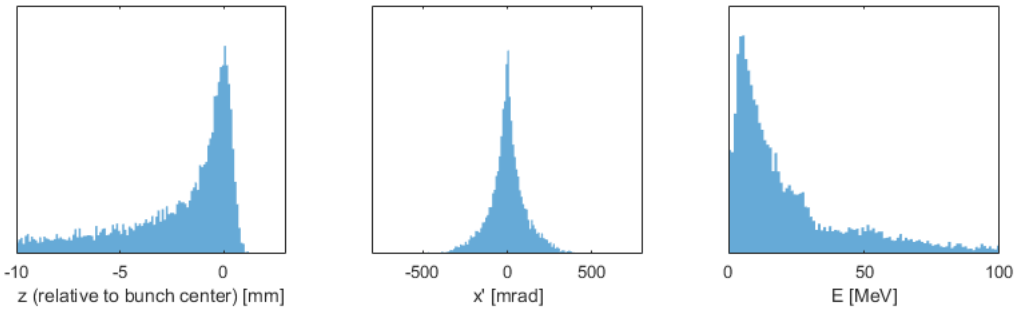

Figure 28: Positron distribution at the input of the first RF cavity.

As previously mentioned, a small longitudinal emittance is key to a large yield at the damping ring. Namely, the phase tuning of the RF cavities must not only seek for a high capture efficiency, but also to concentrate the positrons in a single bucket and reduce their energy spread.

As seen above, two regions in the $(\phi_1,\ \phi_2)$ space provide large yield values by concentrating the positrons in different buckets. Notice that the numeric values of the yield are heavily dependent on the technology (e.g., strength of the solenoid fields, aperture, etc.) and therefore are not presented in Figure 29. A detailed overview of both working points is presented in Figures 31 and 32.

It is clearly shown above how both working points can provide a very high capture efficiency and concentrate a large part of the positrons in one single bucket. However, using the second bucket has some additional advantages. First, the first cavity is tuned with a decelerating mode (see reference energy plot in Figure 32), which is a widely used technique in positron sources for reducing the energy spread (compare energy profiles in Figures 31 and 32) and improve the yield [24]. In addition, this working point is at a very stable region of the $(\phi_1,\ \phi_2)$ space (See "second bucket" in Figure 29) and also

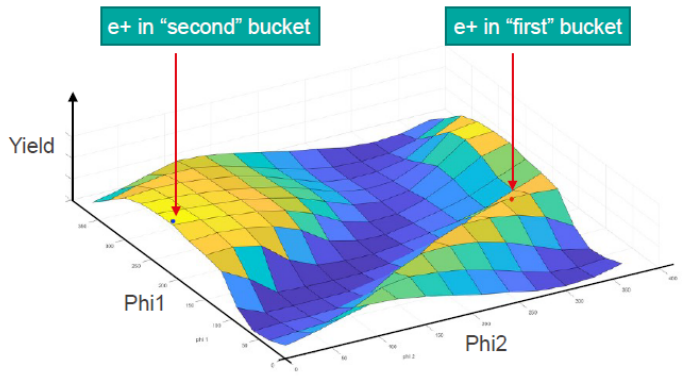

Figure 29: Sweep of the phases of first (ϕ_1) and second (ϕ_2) cavity.

draws less electrons to the main bucket, which could eventually compromise the time structure measurement with the fast BPM.

5.5 Solenoids Around the RF Structures

Due to the extremely high emittance of the positrons, a strong and uniform magnetic field along the cavities is required to maintain the beam confinement. Such field is produced by two solenoids surrounding each structure, as seen in Figure 30.

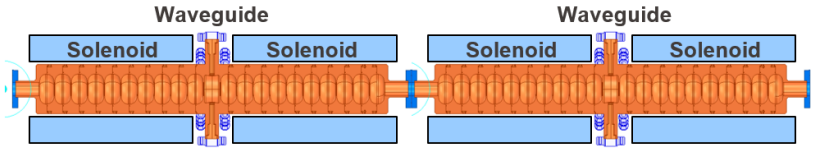

Figure 30: Schematic view of 4 solenoids surrounding the SW cavities.

These solenoids act as continuation of the AMD, and heavily determine the acceptance of the system. Studies by Helm [19] point out that, in cylindrical coordinates, the maximum acceptance in r and θ are given by:

$$r_{max} = \sqrt{\frac{B_s}{B_o}}\, a \tag{1}$$

$$\theta_{max} = \sqrt{\frac{B_s\ B_o}{P_o}}\, a \tag{2}$$

Where B0 is the peak field of the AMD, BS the field of the solenoids around the cavities, a the iris aperture and P0 the scalar momentum of the particle of lowest energy. From the equations above it can be derived that high B0 values will also require relatively high BS. In our particular case, the use of a multi-Tesla field for the AMD implies that strong solenoids are required around the cavities.

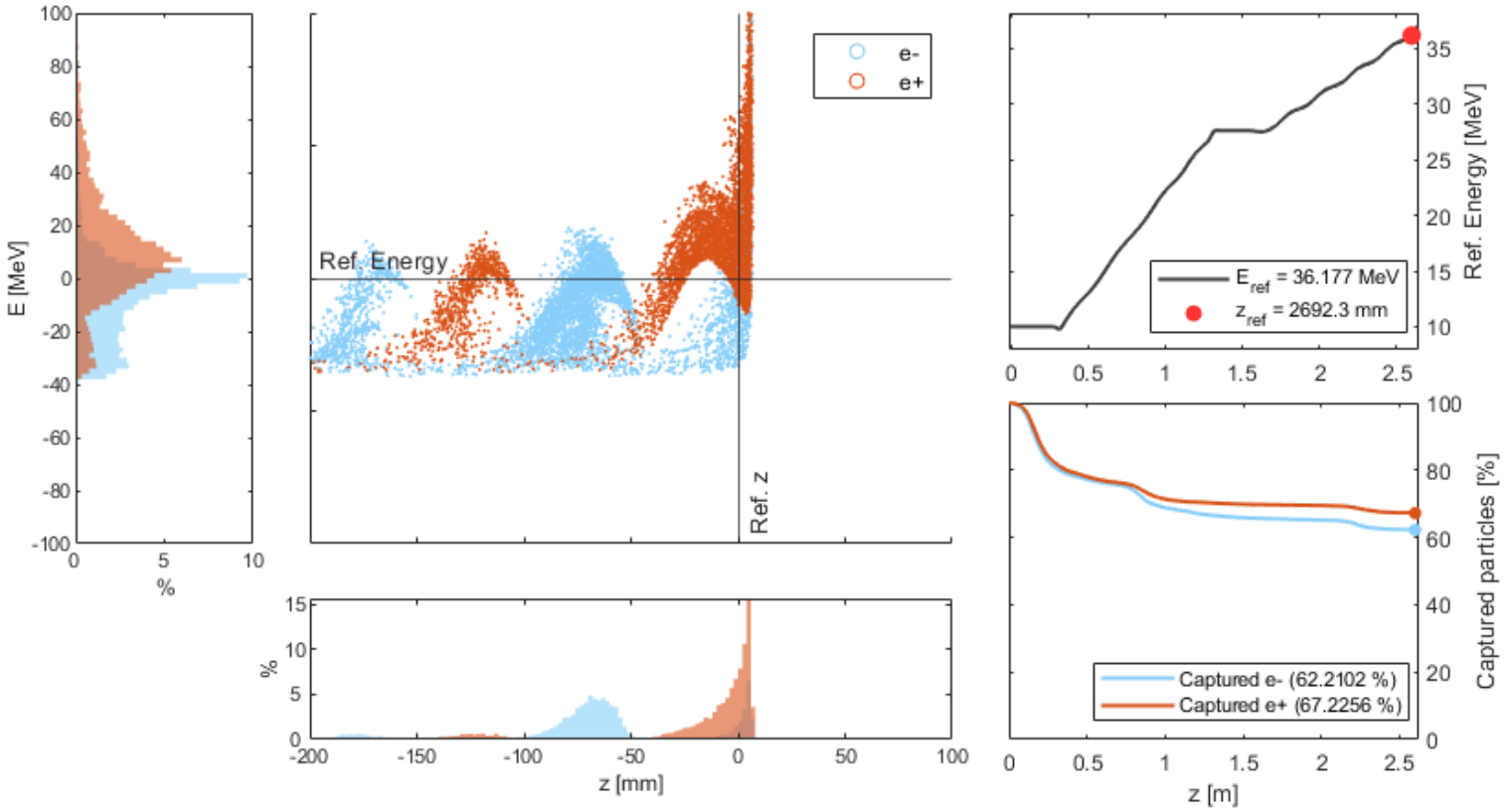

Figure 31: Positron charge concentrated in first bucket. The plots on the left represent the electron (blue) and positron (red) distribution at the output of second cavity. On the right, the bunch center energy and capture efficiency evolution along z are plotted.

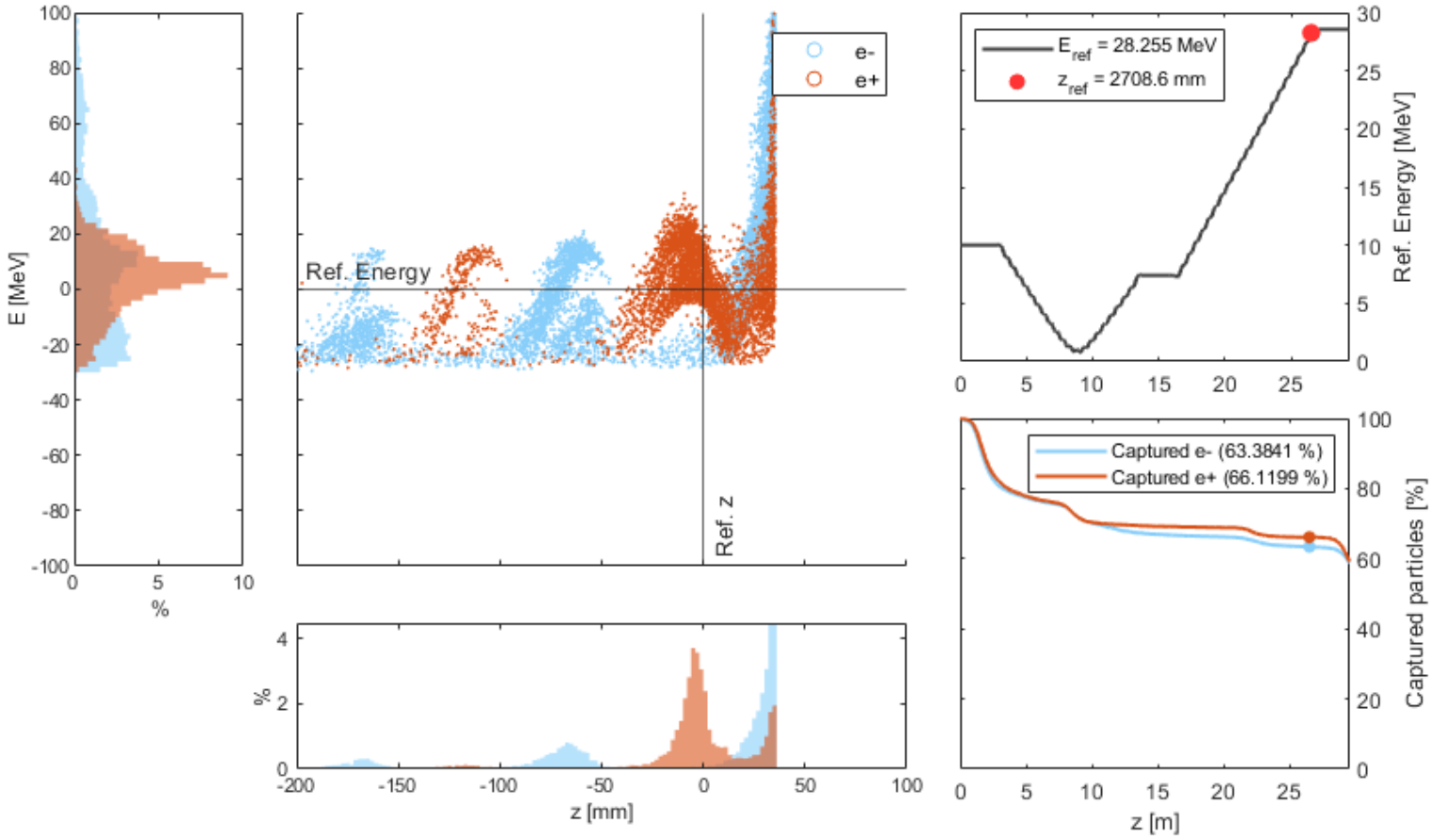

Figure 32: Positron charge concentrated in second bucket.

5.5.1 Normal Conducting vs. Superconducting Technology

The technology of such solenoids is still under discussion. On the one hand, it is possible to achieve relatively strong magnetic fields (0.3 – 0.7 T) with normal conducting (NC) solenoids, which can nevertheless lead to an extreme power consumption. As seen in Table 11, four 0.5 T and 0.7 T NC solenoids would require around 5- and 10-times higher power than the two SW cavities respectively. Therefore, 0.3 T is adopted as reference working point for the NC case as it is the only practical solution.

Table 11: Power consumption of different NC solenoid arrangements compared to SW cavities.

x4 0.3 T NC solenoids	48 kW
x4 0.5 T NC solenoids	136 kW
x4 0.7 T NC solenoids	268 kW
x2 SW Cavities	26 kW[1]

[1]Assuming operation at 100 Hz and 40% klystron efficiency

On the other hand, superconducting (SC) solenoids can provide stronger fields (1 – 2 T) even at large apertures with no need of high voltages [25]. Also, it is shown in Figure 33 how field values in the SC region lead to extremely high capture efficiency. The value of 1.5 T is chosen as second reference point for the SC option, as a good trade-off between yield and cost. One can notice how the use of SC increases the capture efficiency by almost a factor 3 with respect to NC.

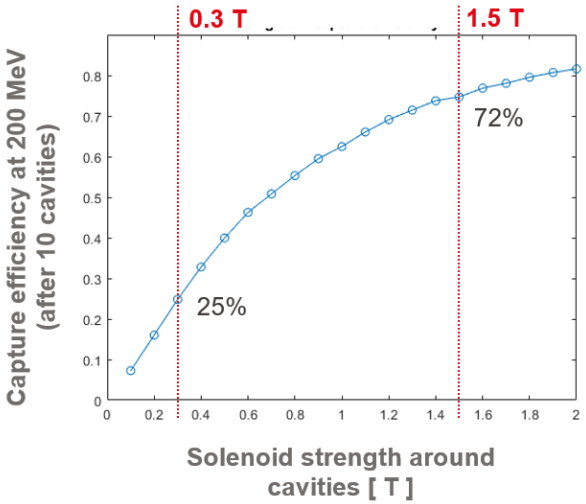

Figure 33: Relation between the capture efficiency and the solenoid strength.

5.5.2 Current Baseline Solution: Nb-Ti

SC technology is adopted as first option for the P-cubed solenoids, and delivering a feasible design proposal has been one of the highest priorities. To this respect, Niobium-Titanium alloy (Nb-Ti) coils have been suggested as most suitable technology. Despite Nb-Ti being a low temperature SC, it can provide fields in the desired range (1 — 2 T) at a relatively moderate cost. Also, it is expected that the size of the cryostat will not conflict the required, very small coil separation [26].

In Figure 30, the current baseline design of the solenoids around the P-cubed structures is presented. In order to provide a higher field flatness, notched coils are introduced in the ends of principal solenoids. This effect is clearly noticeable in the Figure 34, showing the contribution of the principal and notched coils in grey dashed curves, and the effective field of a single solenoid in solid grey curves. The red curve on top represents the combined field, where a flatness is very noticeable.

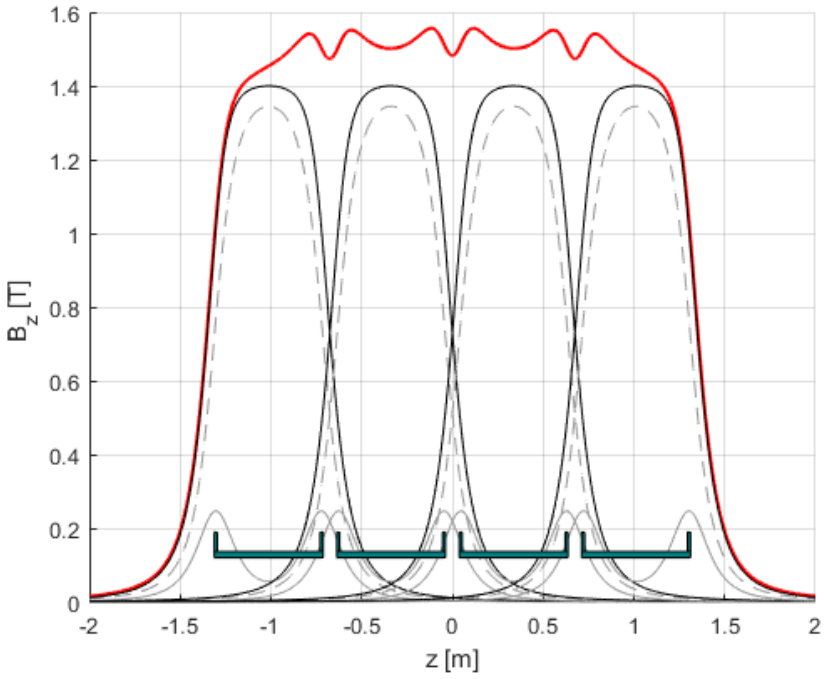

Figure 34: On-axis field produced by the baseline SC solenoid design, including a sketch of the coil dimensions and the contribution of single coils.

5.5.3 Field Flatness Study

The distance between the solenoids is a critical parameter, and several mechanical constraints like the RF coupler waveguide size or the distance between cavities need to be taken into account. In Figure 35, the importance of a flat field is exemplified. On the left, the solenoid layout shown in Figure 34 is tested along 10 cavities in a beam dy-

namics simulation. Notice how little or no losses occur as of the first 2 meters of the linac. In contrast, the plot on the right shows the same magnet arrangement with an intentionally large separation between cavities. Notice how every time the solenoid field drops, the beam confinement stops and significant losses occur.

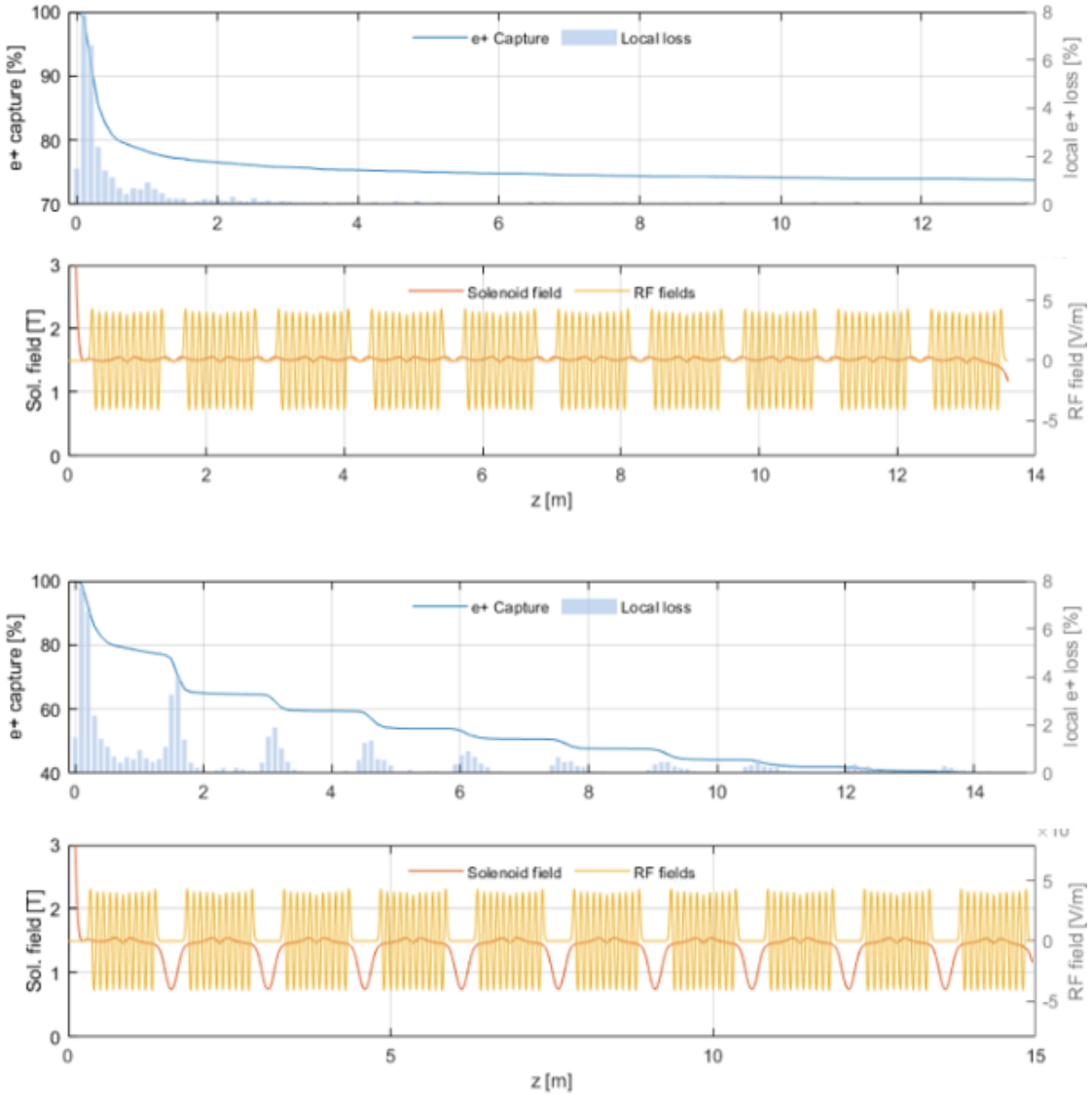

Figure 35: Beam dynamics simulations of solenoid arrangements providing better (top) and worse (bottom) field flatness. Top plots: capture efficiency and local losses. Bottom plots: the RF and solenoid field profiles on axis.

References

[1] M. Benedikt et al., *Future Circular Collider: Conceptual Design Report Vol. 2*, CERN-ACC-2018-0057, accepted for publication in EPJ ST (2018), `https://fcc-cdr.web.cern.ch/#FCCEE`.

[2] K. Akai, K. Furukawa, and H. Koiso, *Superkekb collider*, Nuclear Instruments and Methods in Physics Research Section A: Accelerators, Spectrometers, Detectors and Associated Equipment, 907:188–199, 2018.

[3] `https://indico.cern.ch/event/1047479/`

[4] J. E. Clendenin et al. *SLC positron source startup*, in 14th International Linear Accelerator Conference, 9 1988.

[5] O. Salim et al., *Overall Injection Strategy for FCC-ee*, `http://dx.doi.org/10.18429/JACoW-eeFACT2018-TUPAB0`.

[6] S. Bettoni et al., *Low emittance injector design for free electron lasers*, Phys. Rev. ST Accel. Beams, 18:123403, Dec 2015.

[7] C. Bayar et al., *Design and optimisation of the positron production chain for CLIC from the target to the damping ring*, NIM A 869 (2017) 56-62.

[8] A. Latina, *RF-Track Reference Manual*, CERN, Geneva, Switzerland, June 2020, DOI: 10.5281/zenodo.3887085.

[9] J.-Y. Raguin, Private communication, April 2022.

[10] I. Chaikovska et al., *Positron sources: from conventional to advanced accelerator concepts-based colliders*, prepared for submission to JINST, 10 Feb 2022.

[11] A. Variola. *Advanced positron sources*, Nuclear Instruments and Methods in Physics Research Section A: Accelerators, Spectrometers, Detectors and Associated Equipment, 740:21–26, 2014. Proceedings of the first European Advanced Accelerator Concepts Workshop 2013.

[12] 8. V. N. Baier, V. M. Katkov, and V. M. Strakhovenko, *Electromagnetic processes at high energies in oriented single crystals*, World Scientific, 1998.

[13] R Chehab, F Couchot, AR Nyaiesh, F Richard, and X Artru, *Study of a positron source generated by photons from ultrarelativistic channeled particles*, in Proceedings of the 1989 IEEE Particle Accelerator Conference, 1989, pages 283–285.

[14] Y. Zhao et al., *Comparison of different matching device field profiles for the FCC-ee positron source*, Proceedings of the 12th IPAC, Campinas, Brazil, 2021, doi:10.18429/JACoW-IPAC2021-WEPAB015.

[15] R. Chehab, *Positron Sources*, in CAS: 5th General Accelerator Physics Course, Jyvaskyla, Finland, 1992, pp.643-678.

[16] I. Chaikovska et al., *Positron Source for FCC-ee*, in 10th Int. Particle Acc. Conf., Melbourne, Australia, pp. 424-427.

[17] *Geant4: A simulation toolkit. Book for application developers*, v. 11.0, CERN, Geneva, 2011.

[18] *A space charge tracking algorithm*, v. 3.2, DESY, Hamburg, 2017..

[19] R. Helm, *Adiabatic Approximation for Dynamics of a Particle in the Field of a Tapered Solenoid*, SLX-4, 1962.

[20] J. Chehab et al., *An adiabatic matching device for the Orsay linear positron accelerator*, in IEEE Transactions on Nuclear Science, Vol. NS-30, No. 4, August 1983.

[21] Y. Iwasa, *HTS Magnet*, in Case studies in superconducting magnets, 2nd ed. Boston: Springer, 2009, pp. 587-589.

[22] Y. Zhao, J. Kosse, private communication, 2021.

[23] Y. Zhao, private communication, 2021.

[24] B. Aune, R. Miller, *New Method for Positron Production at SLAC*, in 1979 Linear Accelerator Conference proceedings, Montauk, New York, US, pp. 440-443.

[25] J. Kosse, private communication, 2022.

[26] J. Kosse, private communication, 2022.

Publications and Conference Contributions

- Y. Zhao et al., Comparison of different matching device field profiles for the FCC-ee positron source, 12th Int. Particle Acc. Conf. IPAC2021, Campinas, SP, Brazil, doi:10.18429/JACoW-IPAC2021-WEPAB015.
- N. Vallis et al., P-cubed: the FCC-ee e+ source demonstrator at SwissFEL, under preparation.
- P. Craievich et al., FCC-ee Injector Complex studies, under preparation.
- Contributions to the FCC week 2022 (30.05-03.06): https://indico.cern.ch/event/1064327
  - Overall layout and parameter summary, Paolo Craievich (PSI)
  - Electron Beam dynamics in linacs, Simona Bettoni (PSI)
  - Positron Beam dynamics in linac1, Mattia Schaer (PSI)
  - RF design of the linacs, Hermann Pommerenke (CERN)
  - Positron capture simulations of the FCC-ee positron source", Contributor: Yongke Zhao (CERN)
  - Radiation environment and shielding simulations for the FCC-ee positron source, Barbara Humann (CERN)
  - HTS solenoid for positron source experiment at PSI,Michal Duda (PSI)
  - Damping ring design, Antonio De Santis (INFN)
  - Transfer Lines design, Rebecca Ramjiawan (CERN)
  - PSI Positron production (P-cubed) project in SwissFEL, Nicolas Vallis (PSI)
- CHART workshop at PSI (09.06): https://indico.psi.ch/event/12727/
- Annual meeting of the Swiss Physical Society (27.06-30.06), contribution in Applied Physics and Plasma Physics session: The P-cubed project, Mattia Schaer.
- ICHEP conference (06.07-13.07): https://www.ichep2022.it, Fcc-ee Injector studies, Paolo Craievich
- IPAC 2022 (12.6-17.7.2022): https://www.ipac22.org/
  - B. Humann et al., Radiation Load Studies for the FCC-ee Positron Source with a Superconducting Matching Device, poster contribution
  - P. Craievich et al., FCCee Injector studies
  - S. Ogur et al., Target Studies for the FCC-ee Positron Source
  - Y. Zhao et al., Optimisation of the FCC-ee Positron Source Using a HTS Solenoid Matching Device

  - O. Etisken et al., Collective Effects Estimates for the Current Damping Ring Design of the FCC-e+e-

- Linac conference 2022 (28.08-02.09) `https://linac2022.org/`
  - H. W. Pommerenke et al., RF design of traveling-wave accelerating structures for the FCCee injector complex
  - M. Schaer et al., Linac Design To Boost The Energy Of The Very Large Emittance Positron Bunch Up To 1.5 GeV In The FCC-ee Injector Complex
  - N. Vallis et al., The PSI Positron Production project
  - S. Doebert et al., Electron Sources for FCC Injector

Collaborators

PSI:	P. Craievich, B. Auchmann, I. Besana, S. Bettoni, H. Braun, M. Duda, E. Hohmann R. Ischebeck, P. Juranic, J. Kosse, G. L. Orlandi, M. Pedrozzi, J.-Y. Raguin, S. Reiche, S. Sanfilippo, M. Schaer, N. Vallis, R. Zennaro
IJCLab:	I. Chaikovska, S. Ogur
CERN:	A. Grudiev, W. Bartmann, M. Benedikt, T. Brezina, M. Calviani, S. Doebert, Y. Duthell, O. Etisken, B. Humann, A. Latina3, , A. Lechner, H. Pommerenke R. Ramjiawan, Y. Zhao, F. Zimmermann
INFN-LNF:	C. Milardi, O. Blanco, A. De Santis
KEK:	K. Oide, Y. Enomoto, K. Furukawa
BINP:	P. Martyshkin